https://doi.org/10.5194/se-2021-76
Preprint. Discussion started: 11 June 2021

Solid Earth Discussions

Structural complexities and tectonic barriers controlling recent seismic activity of the Pollino area (Calabria-Lucania, Southern Italy) - constraints from stress inversion and 3D fault model building

Daniele Cirillo[1-2]*, Cristina Totaro[2-3], Giusy Lavecchia[1-2], Barbara Orecchio[2-3], Rita de Nardis[1-2], Debora Presti[2-3], Federica Ferrarini[1-2], Simone Bello[1-2] and Francesco Brozzetti[1-2]*

[1] Università degli studi "G. d'Annunzio" Chieti-Pescara, DiSPUTer, via dei Vestini 31, 66100 Chieti, Italy.
[2] CRUST Centro inteRUniversitario per l'analisi SismoTettonica tridimensionale, Italy.
[3] Università degli studi di Messina, Dipartimento di Scienze Matematiche e Informatiche, Scienze Fisiche e Scienze della Terra -Viale F. Stagno D'Alcontres, 98166, Messina, Italy

Correspondence to: d.cirillo@unich.it; francesco.brozzetti@unich.it

Abstract. The integration of field geology and high-resolution seismological data allowed us to reconstruct the 3D Fault Model of the sources which gave rise to the 2010-2014 Pollino seismic sequence.

The model is constrained at the surface by structural geological data which provide the true attitude of the single faults and their cross-cut relationships. At depth, the fault geometry was obtained using the distributions of selected high-quality relocated hypocenters. Relocations were carried out through a non-linear Bayloc algorithm, followed by the double-difference relative location method HypoDD, applied to a 3D P-wave velocity model.

Geological and seismological data converge in describing an asymmetric active extensional fault system characterized by an E to NNE-dipping low-angle detachment, with its high-angle synthetic splays, and SW- to WSW-dipping, high-angle antithetic faults.

The cluster of hypocenters and the peculiar time-space evolution of the seismic activity highlight that two sub-parallel WSW-dipping seismogenic sources, namely the Rotonda-Campotenese and Morano-Piano di Ruggio faults activated during the seismic crisis.

By applying to the activated structures the appropriate earthquake-scaling relationships, based on fault length and fault area, we infer that the maximum expected magnitudes calculated using the fault area are the more reliable. We estimated M_w=6.4 for the Rotonda-Campotenese and M_w=6.2 for the Morano-Piano di Ruggio deducing that both the faults did not release their seismic potential during the 2010-2014 seismic sequence.

The size of the activated patches, reconstructed by projecting on the 3D seismogenic fault planes the early aftershocks of the seismicity clusters, are consistent with the observed magnitude of the associate strongest events.

https://doi.org/10.5194/se-2021-76
Preprint. Discussion started: 11 June 2021


Solid Earth Discussions

Finally, we point out that the western segment of the Pollino Fault, despite not being presently active, acts as a barrier to the southern propagation of the Rotonda-Campotenese and Morano-Piano di Ruggio faults, limiting their dimensions and seismogenic potential.

1 Introduction

In recent years, the reconstruction of 3D Fault Models (hereinafter referred to as 3DFM) of potentially seismogenic structures has become an increasingly practiced methodology in the seismotectonic analysis of regions undergoing active deformation (SCEC, 2021; Lavecchia et al., 2017; Castaldo et al., 2018; Di Bucci et al., 2021). The techniques to obtain the 3DFM integrate all the available surface ad subsurface data and allow to reconstruct the 3D geometry of seismogenic structures. In particular, detailed structural-geological data are used to define the geometry of the active faults at the surface whereas high-quality geophysical data are needed to constrain the shape of the sources at depth. If these conditions are met, 3DFM reconstruction allows determining the spatial relationships and the interactions between adjacent sources and identifying any barriers hampering at depth the propagation of the coseismic rupture. Moreover, such an approach leads to estimate with great accuracy the area of the seismogenic fault and the associated expected magnitude.

In Italy, reconstruction of 3DFM could give important achievements in the Apennine active extensional belt which is affected by significant seismic activity (ISIDe, 2007; Rovida et al., 2020). This belt consists of ~NW-SE striking Quaternary normal fault systems, and the related basins, located just west or within the culmination zone of the chain (Calamita et al., 1992; Brozzetti and Lavecchia, 1994; Lavecchia et al., 1994, 2021; Barchi et al., 1998; Cinque et al., 2000; Brozzetti, 2011; Ferrarini et al., 2015). Its structural setting is very complicated due to a polyphase tectonic history characterized by the superposition of Quaternary post-orogenic extension on Miocene-Early Pliocene folds and thrusts and on Jurassic-Cretaceous sin-sedimentary faults (Elter et al., 1975; Ghisetti and Vezzani, 1982, 1983; Lipmann-Provansal, 1987; Patacca and Scandone, 2007; Mostardini and Merlini, 1986; Vezzani et al., 2010, among others).

Since the beginning of the Pleistocene, regional normal fault systems dissected the contractional structures with displacements that locally reach some km. Over time, detailed structural geological studies made it possible to recognize several seismogenic faults in the Apennine active extensional belt (Barchi et al., 1999; Galadini and Galli, 2000; Maschio et al., 2005; Brozzetti, 2011) and, in some cases, to document, through paleo-seismological data, their timing of reactivation during the Holocene (Galli et al., 2020). Furthermore, in recent years, new technologies have made it possible to reconstruct fault patterns with very high precision, thus allowing to constrain the fault structures at the surface at sub-meter scale resolution (e.g., Westoby et al., 2012; Johnson et al., 2014; Cirillo, 2020; Bello et al., 2021b). Accurate geophysical prospections (e.g., ground Penetration Radar), aimed at the study of historical earthquakes' surface faulting, allowed to investigate the sub-surface (e.g., Gafarov et al., 2018; Ercoli et al., 2013, 2021), but high-resolution only providing constraints at shallow depths (few tens of m).

Conversely, the geometries of the faults at depth are poorly reliable since deep geological and geophysical constraints are often lacking.

https://doi.org/10.5194/se-2021-76
Preprint. Discussion started: 11 June 2021

In fact, in the last decades, seismic reflection prospecting and deep-well exploitation for hydrocarbon research, avoided the area affected by active extension, and focused on the eastern front of the chain and on the Adriatic-Bradanic foreland basin system (ViDEPI: www.videpi.com).

The availability of high-resolution seismological datasets, to be integrated with geological ones, provides a new opportunity to image the tri-dimensional shape of the sources.

Datasets characterized by highly precise re-locations of hypocenters were collected during recent seismic sequences associated with medium- and high-magnitude earthquakes (Chiaraluce et al., 2004, 2005, 2011, 2017; Totaro et al., 2013, 2015). These sequences include thousand of earthquakes in confined rock volumes which appear to roughly connect with the fault traces mapped at the surface. Therefore, such distributions of earthquakes are generally referred to as ongoing rupture processes affecting an entire, or wide portion of, seismogenic faults.

In some cases, (Chiaraluce et al., 2017; Valoroso et al., 2017) very high-resolution hypocenter locations, as well as reflection seismic lines, allow to clearly highlight the seismogenic structures at depth (Lavecchia et al., 2011, 2012, 2015, 2016).

A number of favourable factors make the Calabria-Lucania boundary (southern Apennines) an -interesting study area for the reconstruction of 3DFM, using good quality seismological data.

This area includes the northern sector of the so-called “Pollino seismic gap” (Fig. 1), in which paleo-earthquakes up to M=7 are documented (Michetti et al, 1997; Cinti et al., 1997, 2002) whereas the location and size of seismogenic sources are a matter of debate (Michetti et al., 2000; Cinti et al., 2002; Papanikolaou and Roberts, 2007; Brozzetti et al., 2009, 2017a).

Recently, using structural-geological and morpho-structural survey techniques, Brozzetti et al. (2017a) mapped a set of active faults between the Mercure, Campotenese, and Morano Calabro Quaternary basins (Fig. 1a).

During the 2010-2014 time interval, this area was affected by a low to moderate instrumental seismicity (Pollino seismic sequence), climaxing at the 25 October 2012, M_w 5.2 Mormanno earthquake, with thousands of recorded events (Totaro et al., 2013, 2015). During the sequence, two other strongest events occurred close to the village of Morano Calabro: the 28 May 2012 (M_w 4.3), and the 6 June 2014 (M_w 4.0) earthquakes (Fig. 1b).

The whole seismicity was arranged in two major clusters and a minor one (Totaro et al., 2015). Each major cluster was associated with one strong event and was generated by an independent seismogenic structure (Brozzetti et al., 2017a).

The pre-existence of a seismic network, that was implemented after the start of the sequence, made it possible to increase the precision of the hypocentral determination and to relocate the events after an accurate selection, providing a high-quality database (Totaro et al., 2013, 2015; Brozzetti et al., 2017a).

In such context, the main purposes of this work are to:

- reconstruct the 3DFM activated by the Pollino 2010-2014 seismic sequence;
- investigate, at depth, the possible interactions between the various seismogenic sources determining the cross-cut relationships between the faults having different strikes, dip-angles, and timing of activation;
- provide the geometric parameters of the sources aimed at estimating the maximum expected magnitudes based on the defined 3D source.

https://doi.org/10.5194/se-2021-76
Preprint. Discussion started: 11 June 2021

Solid Earth
Discussions
Open Access
EGU

97 Finally, we discuss some methodological aspects which are of general interest for researchers approaching three-
98 dimensional seismotectonics in any structural context. These aspects dwell on the improvements that the proposed
99 procedure provides to the definition of the source model, the limits of the method imposed by the type and quality of the
100 available data, and the possible causes of errors with the relative ranges of variation.

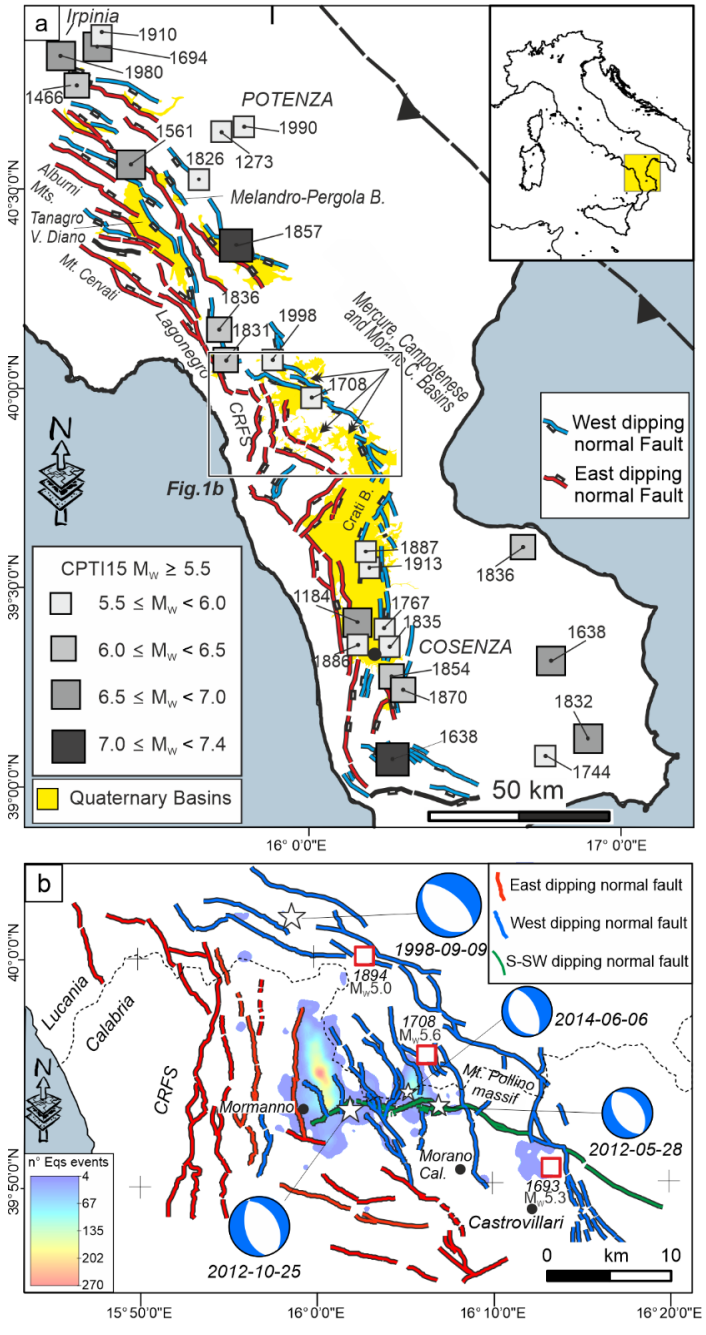

101

https://doi.org/10.5194/se-2021-76
Preprint. Discussion started: 11 June 2021

Figure 1: Seismotectonic context of the study area. (a) Active faults of the Southern Apennines with major historical and instrumental earthquakes from Parametric Catalogue of Italian Earthquakes, CPTI15 v3.0 (Rovida et al., 2020, 2021). (b) Distribution of the 2010-2014 Pollino seismic sequence focal mechanisms are the events with Mw>4.0 (Totaro et al., 2015, 2016). Normal faults between the Mercure, Campotenese, Morano Calabro and Castrovillari Quaternary basins are reported (after Brozzetti et al., 2017a).

2 Seismotectonic framework

2.1 Geological Setting

The Mt. Pollino massif is located at the Calabrian-Lucanian boundary (Fig. 1) in a sector of the Apennines structured during the Middle-Late Miocene contractional tectonics that affected the western Adria Plate (D'Argenio, 1992; Patacca and Scandone, 2007; Ietto and Barilaro, 1993; Iannace et al. 2004, 2005, 2007).

The surface geology in this area is characterized by the superposition of two main tectonic units each derives from different paleogeographic domains. These are represented, from bottom to top, by:

– the "Apenninic" units (or “Panormide”), characterized by carbonate platform, including the Verbicaro and Pollino Units with an age from Triassic to Early Miocene, locally intruded by basaltic rocks (Ogniben, 1969, 1973; Amodio-Morelli et al., 1976; Iannace et al., 2007; Patacca and Scandone, 2007; Vezzani et al., 2010; Tangari et al 2018);

– the "Ligurian" units, that consist of ophiolites and deep-sea sedimentary deposits derived from the Western Tethys oceanic basin (Ogniben, 1969, 1973; Amodio-Morelli et al., 1976; Liberi et al., 2006; Liberi and Piluso, 2009; Filice et al., 2015).

During uppermost Miocene-Pliocene times, the folds and thrusts edifice was displaced by WNW-ESE-striking left-lateral wrench faults, among which, the Pollino fault (POL) played an important role (Fig. 1b) (Grandjacquet, 1962; Ghisetti and Vezzani; 1982; Van Dijk et al., 2000).

Subsequently, regional-scale extensional faults systems, consisting of E- and W-dipping conjugate normal faults, dissected the Tyrrhenian side and the core of the orogen which assumed a typical basin and range relief.

The Quaternary extensional phase also caused the reactivation of the previous strike-slip structures. In particular, the reactivation of the POL, with normal to normal-oblique kinematics, has been documented at least since the Early-Middle Pleistocene (Ghisetti and Vezzani, 1982, 1983, Brozzetti et al., 2017a).

Actually, the age of onset of the extensional tectonic is still under discussion; it is referred by some authors to the Early Pleistocene (Ghisetti and Vezzani, 1982; Schiattarella et al., 1994; Papanikolaou and Roberts 2007; Barchi et al., 2007; Amicucci et al., 2008; Brozzetti, 2011; Robustelli et al., 2014), whereas it would not be older than the Middle Pleistocene, according to others (Caiazzo et al., 1992; Cinque et al. 1993; Hypolite et al., 1995; Cello et al., 2003; Giano et al., 2003; Spina et al., 2009; Filice and Seeber, 2019).

In the Campania-Lucania and north-Calabria sectors of the southern Apennines, the active extensional belt includes three main

https://doi.org/10.5194/se-2021-76
Preprint. Discussion started: 11 June 2021

alignments of normal faults and Quaternary basins, arranged in a right-lateral en-echelon setting (Fig. 1a). From north to south they are: i) northern alignment: including the Irpinia fault and the Melandro-Pergola and Agri basins; ii) intermediate alignment: developing from the Tanagro-Vallo di Diano basins to the Mercure-Campotenese and Morano Calabro basins, and iii) southern alignment: from the Castrovillari fault to the southern Crati basin (Pantosti and Valensise, 1990, 1993; Ascione et al., 2013; Galli and Peronace, 2014; Ghisetti and Vezzani, 1982, 1983; Barchi et al., 1999, 2007; Blumetti et al., 2002; Amicucci et al., 2008; Maschio et al., 2005; Villani and Pierdominici, 2010; Brozzetti, 2011, Faure Walker et al., 2012; Brozzetti et al., 2009, 2017a, 2017b; Robustelli et al., 2014; Sgambato et al., 2020; Bello et al., 2021a).

All along the above alignments, the geometry and kinematics of the major normal faults are kinematically compatible with a SW-NE direction of extension (Maschio et al. 2005; Brozzetti, 2011; Brozzetti et al., 2009; 2017a). A similar orientation of the T-Axis is obtained from the focal mechanisms of the major earthquakes from CMT and TDMT databases (Pondrelli et al., 2006; Scognamiglio et al., 2006; Montone et al., 2012; Totaro et al., 2016) and from GPS data (D'Agostino et al., 2014). Cheloni et al. (2017) demonstrated, from geodetic GPS and DInSAR analysis, that the Pollino area was affected by important deformation rates during the 2010-2014 seismic activity, with increasing and decreasing of slip values due to the temporal and spatial behavior of the recorded seismicity (Passarelli et al. 2015). The present activity of these normal faults systems is firstly suggested by the control exerted on the distribution of seismicity, as shown by the location of upper crustal instrumental earthquakes (ISIDe database, Working Group INGV; Brozzetti et al., 2009; Totaro et al., 2014, 2015; Cheloni et al., 2017; Napolitano et al., 2020, 2021; Pastori et al., 2021) and of destructive historical events (Fig. 1, Rovida et al., 2021).

The area affected by the 2010-2014 seismicity extends from the Mercure basin to the Campotenese and Morano Calabro basins that are along the intermediate extensional fault-alignment described above. In this area, recent structural-geological works highlighted three main sets of genetically-linked normal and normal-oblique active faults (Brozzetti et al., 2017a; Figs 1b, 2). The first one, E- to NNE-dipping, referred to as the Coastal Range Fault Set (CRFS; red lines in Figs 1b, 2) encompasses four sub-parallel major fault segments which, from west to east are: Gada-Ciagola (GCG), Papasidero (PPS), Avena (AVN) and Battendiero (BAT) faults. Their strike-direction varies southward from N-S to WNW-ESE.

The other two sets strike ~NW-SE, and dip ~SW (blue lines in Figs 1b, 2). The western one, developing from Rotonda to Campotenese villages through the 2010-2014 seismic sequence epicentral area, consists of two main right-stepping en-echelon fault segments. They are referred to as ROCS system, and include the Rotonda-Sambucoso (RSB) and Fosso della Valle-Campotenese (VCT; Fig.1b). The eastern set, including the en-echelon Castello Seluci-Piana Perretti-Timpa della Manca (CPST), the Viggianello-Piano di Pollino (VPP) and the Castrovillari (CAS) faults, represents the break-away zone of the Quaternary extensional belt. In the area between these two W-dipping sets, the W to NW-dipping Morano Calabro-Piano di Ruggio (MPR) and Gaudolino (GDN) faults, show evidences of Late Quaternary activity (Brozzetti et al., 2017a; Fig. 1b).

https://doi.org/10.5194/se-2021-76
Preprint. Discussion started: 11 June 2021


Solid Earth Discussions

2.2 Earthquake/fault association and kinematics of the 2010-2014 seismic sequence

In the study area, the POL and the adjacent CAS faults (Fig. 1b) are the most studied structures from the seismotectonic point of view, as, based on the results of paleoseismological investigations (Michetti et al., 1997, 2000; Cinti et al., 1997, 2002), they are considered active and capable of producing strong earthquakes and surface faulting. In fact, according to the aforementioned literature, both the faults were associated with at least two strong earthquakes, (M 6.5 and M 7.0), occurred in 2000-410 B.C. and 500-900 A.D.

The epicenter of the 8 January 1693 earthquake (Fig. 1b) is also located within the hanging wall block of the CAS and in the footwall block of the MPR fault, some km eastward of the 2012 and 2014 Morano Calabro strong events, then leading to exclude the MPR as the causative fault.

Nevertheless, this event, which was first reported in the CFTI5Med Catalogue (Guidoboni et al., 2018, 2019) with M_w 5.7, was recently reduced to M_w 5.2 (Tertulliani and Cucci, 2014).

The epicenter locations of the M_w 5.5, 1708 (Rovida et al., 2021) and M_w 5.1, 1894 earthquakes, close to the northern termination of the RSB and within its hanging wall, allows hypothesizing the latter fault as the possible seismogenic source.

For what concerns the instrumental seismicity, the main event recorded in the Pollino area is the M_w 5.6 Mercure earthquake (9 September 1998, Fig. 1b), which was followed by some hundred aftershocks. Despite a preliminary attribution to the Castelluccio fault (Michetti et al., 2000), this earthquake was associated by Brozzetti et al. (2009) with the SW-dipping CPST (Fig. 1b), located some km to the NE of the Mercure basin.

The 2010-2014 Pollino seismic sequence was triggered by extensional upper crustal deformations, as highlighted by the focal mechanisms of the three strongest earthquakes (M_w 5.2, 25 October 2012-Mormanno, M_w 4.3, 28 May 2012-Morano Calabro and M_w 4.0, 6 June 2014-Morano Calabro). All the associated WSW-ENE oriented T-axes are also ~parallel to the geological and seismological minimum compression axis provided by the tensorial analysis in the neighboring Mercure area (Brozzetti et al., 2009; Ferranti et al., 2017), or derived from borehole breakout investigations (Montone et al., 2004; Pondrelli et al., 2006), and GPS data (D'Agostino et al., 2014).

The available focal solutions of the Pollino 2010-2014 seismic sequence, display W-dipping seismogenic planes which well correlate with the Quaternary normal fault segments recognized in the epicentral area (see sect. 2.1). The coherence between field and seismological data is even more evident using the dataset provided by Totaro et al. (2015, 2016) and Brozzetti et al. (2017a) which suggest N-S to NNW-SSE-striking, W-dipping, seismogenic sources.

Correlating the hypocenters distribution at depth with the active faults highlighted at the surface, the seismogenic source of the 25 October 2012 Mormanno Earthquake (M_w 5.2), also responsible for the westernmost and larger seismicity cluster (Fig. 1b), is identifiable in both the segments of the WSW-dipping ROCS system (RSB and VCT). These faults dip at surface 70°-75° and would reach, at depth, a dip of ~55° (Brozzetti et al., 2017a).

https://doi.org/10.5194/se-2021-76
Preprint. Discussion started: 11 June 2021

Through similar reasonings, the WSW-dipping MPR fault was suggested to be the causative fault of the eastern, Morano Calabro, cluster (Fig. 1b) and of its two major events (M_w 4.3, 28 May 2012 and M_w 4.0, 6 June 2014). This fault extends for ~7 km in the N170 direction and is co-axial with the W-dipping nodal planes of the two main events of the sequence (Fig. 1b). The partial reactivation of the CAS could be invoked to explain the minor seismicity cluster recorded at the eastern side of the study area, although some of the events seem to be located in its footwall.

3 Material and Methods

3.1 Structural survey and fault kinematic analysis

A series of fieldwork campaigns between 2018 and 2020, were performed to collect fault-slip data in the study and neighbouring areas, at 1:25.000 scale. These measurements were used to integrate the geological-structural data and to constrain the Quaternary extensional faults provided in Brozzetti et al. (2017a). In field, we initially used traditional structural analysis techniques. We integrated the data with data collected through digital mapping, by using the Fieldmove app/software (PetEx Ltd., version 2019.1) installed on a tablet computer. All these data (shown in Fig. 2) were managed in a GIS database elaborated through ArcGIS v.10.8 (ArcMap©). Fig. 2 also shows the location of the kinematic survey sites that are structurally homogeneous outcrops or groups of adjoining outcrops that fall within a maximum distance of 500 m, that is within the diameter of each small circle on the scheme (more detailed localizations in Supplementary Fig. 2).
The overall fault-slip data set was first subdivided in minor and local homogenous kinematic sub-sets represented as pseudo-focal mechanisms using FaultKin 8 software (Marrett and Allmendinger, 1990; Allmendinger et al., 2012) (Fig 3). The obtained beachballs show the computed pseudo-focal mechanism associated with a couple of average fault plane/average slip vector (A.f.p. and A.s.v. respectively, in Fig. 3) obtained through Bingham statistic analysis from the fault population collected in each survey site.
The fault/slip data were subsequently inverted in order to reconstruct the long-term (geological) stress field to be compared with the seismological tensor obtained from available focal mechanisms (see following sec. 3.2). Such comparison allowed verifying the persistence of the stress field over time, at least from the Middle Pleistocene to Holocene times.

3.2 Geological and seismological stress tensor inversion

To investigate the coherence between the geological and the present-day (seismological) stress fields, we applied stress tensor inversions to the available fault-slip data (Fig. 2, 3) and focal mechanisms (Fig. 4).
We used the inversion procedure proposed in Delvaux and Sperner (2003) (Win-Tensor software) and applied it, separately, on the different datasets. The procedure attempts to compute the orientation of the three principal axes of the stress ellipsoid ($\sigma1$, $\sigma2$, $\sigma3$) and the stress ratio $\Phi = (\sigma2-\sigma3)/(\sigma1-\sigma3)$ that optimize the misfit Function (i.e., F5). The latter is built to i) minimize

https://doi.org/10.5194/se-2021-76
Preprint. Discussion started: 11 June 2021

the slip deviation between the observed slip line and resolved shear stress (30° misfit value is not expected to be exceeded), and ii) favor higher shear stress magnitudes and lower normal stress to promote slip on the plane.

The inversion procedure provides for the preliminary (kinematic) analysis of data using an improved version of the Right Dihedron method (Angelier and Mechler, 1977) to determine the starting model parameters (e.g., the reduced stress tensor). The stress ellipsoid is then computed through a 4D grid-search inversion involving several runs during which the reduced tensor is rotated around each stress axis, with a decreasing range of variability (from ±45° to ±5° and the full range of Φ values is checked [0-1]). Each step attempts to find the parameters that minimize misfit function and that are used as a starting point for the next run (see for details Delvaux and Sperner, 2003).

The geological data input consists of 268 quality selected fault/slip data measured along the fault systems of the study area (Fig. 2, 3). During the formal inversion, the same weight value was assigned to each fault giving the same quality factor assigned to the slickenlines.

The seismological data input is represented (initially) by both nodal planes of each focal mechanism; afterward, the plane that is best explained by the stress tensor in terms of the smallest misfit function is considered as the actual fault plane (Delvaux and Barth, 2010).

The inverted seismological data are represented by focal mechanisms ($2.7 \leq M_w \leq 5.0$) taken from Totaro et al. (2015, 2016) and reported in Fig. 4. An exponential weighting factor (corresponding to the earthquake magnitudes) has been assigned to account for the prevailing kinematics of the most energetic events.

The final inversion includes only the fault- and focal-planes that are best fitted by a uniform stress field (Gephart and Forsyth, 1984). The stress inversion results are shown in Fig. 5.

https://doi.org/10.5194/se-2021-76
Preprint. Discussion started: 11 June 2021

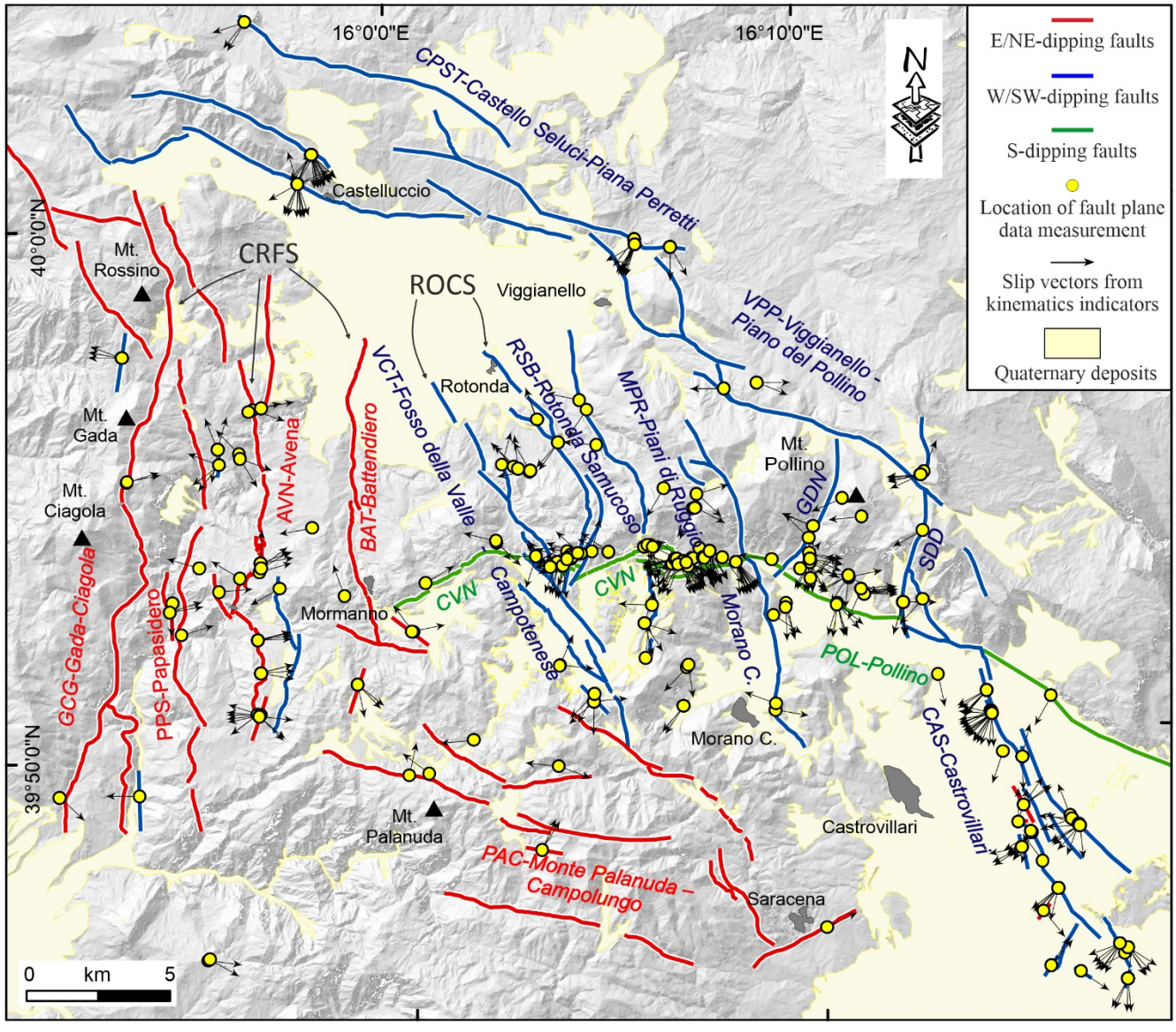

Figure 2: Structural Map at the Calabrian-Lucanian boundary (after Brozzetti et al., 2017a) with location of fault-slip data measurements. Fault Key: CRFS= Coastal Range Fault Set; GCG= Gada-Ciagola fault; PPS= Papasidero fault; AVN= Avena fault; BAT= Battendiero fault; ROCS= Rotonda-Campotenese fault system; VCT= Fosso della Valle-Campotenese fault; RSB= Rotonda-Sambucoso; CVN= Cozzo Vardo-Cozzo Nisco fault; MPR= Morano Calabro-Piano di Ruggio fault; VPP= Viggianello - Piano di Pollino fault; GDN= Gaudolino fault; POL= Pollino fault; CAS= Castrovillari fault; SDD= Serra Dolcedorme fault; PAC= Monte Palanuda – Campolungo fault; CPST= Castello Seluci-Piana Perretti fault.

https://doi.org/10.5194/se-2021-76
Preprint. Discussion started: 11 June 2021

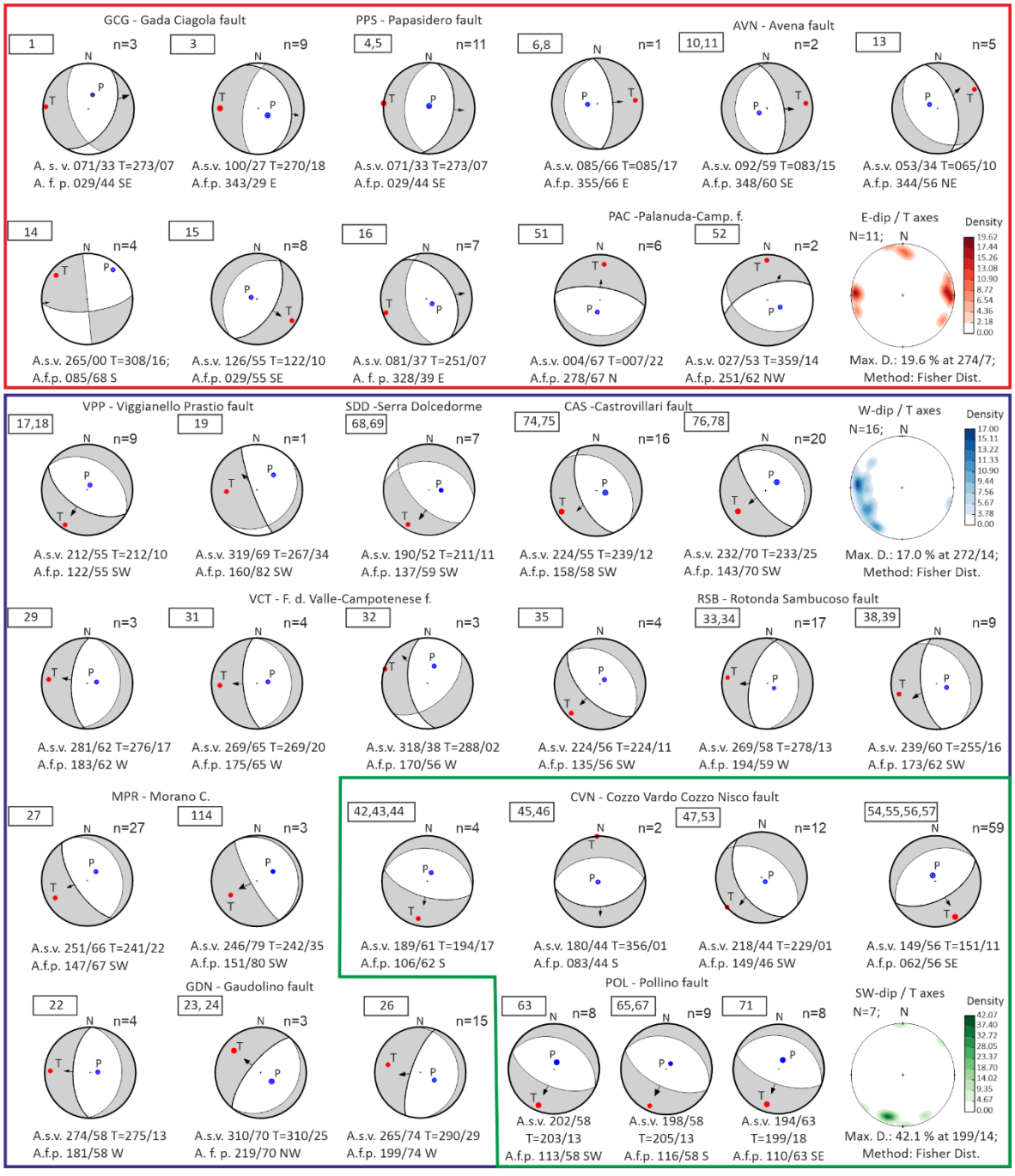

Figure 3: Kinematic analysis and pseudo-focal mechanisms obtained from fault/slip data using the software FaultKin 8 (Allmendinger et al., 2012). Pseudo-focal mechanisms are boxed with different colors on the basis of the fault system to which they belong (color key as in the map of Figure 1, 2). For each fault system the density contour of the T-axis computed for each focal mechanism is reported (lower hemisphere projection). A.s.v.=Average striae value, A.f.p.=Average fault plane. Numbers

https://doi.org/10.5194/se-2021-76
Preprint. Discussion started: 11 June 2021

Solid Earth
Discussions
Open Access
EGU

in the rectangles (top left of each focal mechanism) refer to the group of fault/slip data belonging to or neighbouring of a single site (location in Figure Supplementary 2).

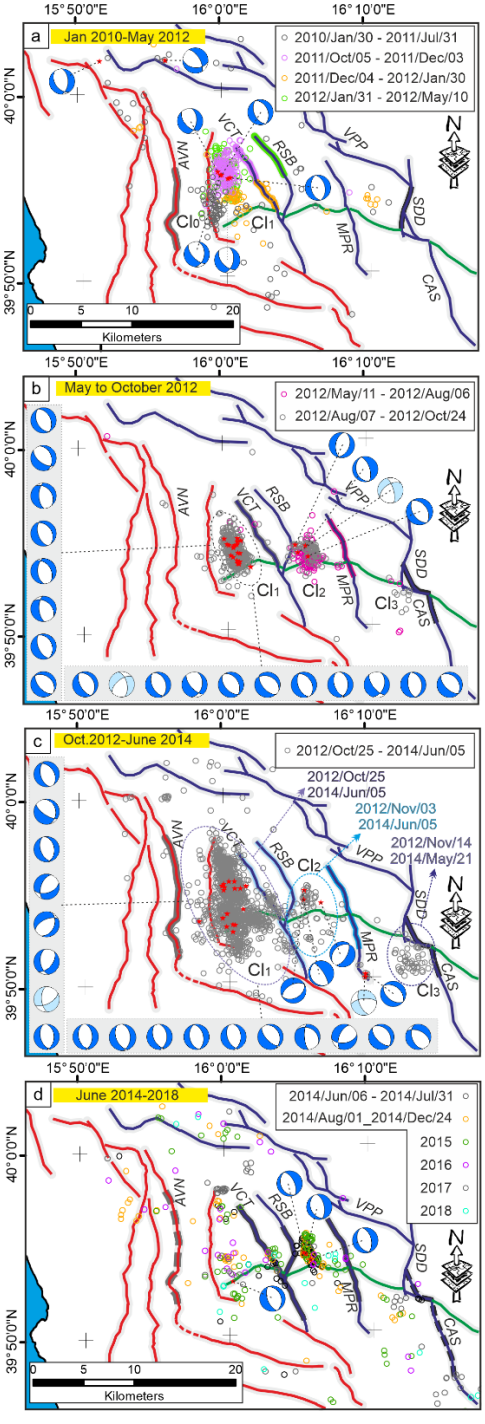

https://doi.org/10.5194/se-2021-76
Preprint. Discussion started: 11 June 2021

Figure 4: Time-space evolution of the 2010-2018 seismic activity in the Pollino area. Each panel shows the distribution of focal mechanisms and epicenters concentrated in a series of neighbouring clusters numbered as Cluster 0, 1, 2, and 3 (Cl0, Cl1, Cl2, Cl3) from west to east according to their activation time. See the main text (section 4.2) for the sequence description.

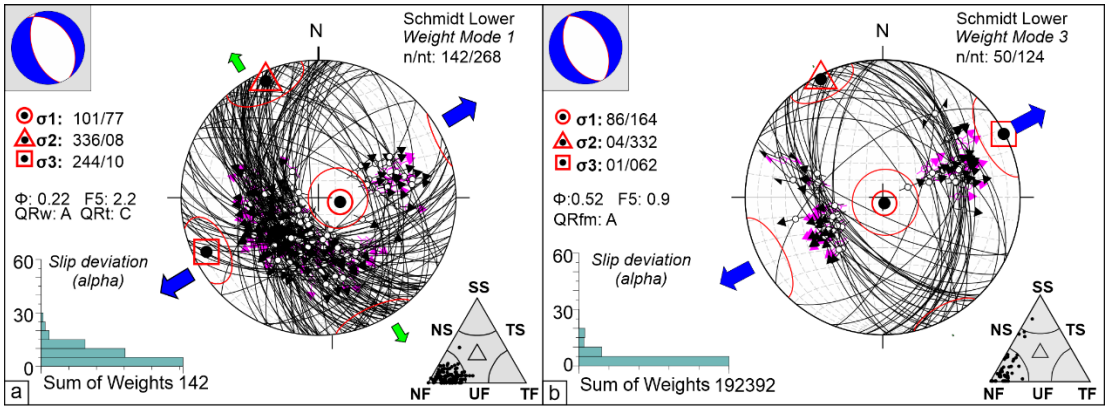

c

Data type	Data (n/nt)	σ1	±1σ	σ 2	±1σ	σ 3	±1σ	Φ	±1σ	QR
Fault/slip vector	142/268	101/77	17.5	336/08	17.9	244/10	16.4	0.22	0.13	A-QRw
Focal mech. nodal planes	50/124	171/87	19.6	332/03	14.8	062/01	19	0.52	0.3	A-QRfm

Figure 5: Stress inversion results for the geological- (a) and seismological (b) data. On the lower hemisphere Schmidt nets, the pairs fault plane/slickenline (a) and focal plane/kinematic indicators (rake) (b) are reported (great circles represent the fault planes; the dark and pink arrows indicate the measured slip directions (or rake) and resolved shears, respectively). The histograms represent the corresponding misfit angles vs. the number of data points; nt = total number of fault data; n = number of successfully inverted fault data; σ1, σ2, σ3 = principal stress axes; Φ = stress ratio = (σ2-σ3)/(σ1-σ3); the quality ranking factors (QR) and the stress inversion parameters with associated uncertainties (1σ standard deviations) are listed in panel (c). On the small upper left nets, the computed stress field represented as a focal mechanism is reported. The triangles reported on the lower right corners of each panel (a) and (b) show the kinematic classification of data according to Frohlich (2001). (c) Geological and seismological stress tensor parameters computed starting from slip-vector measurements collected along the investigated fault systems (Figs. 2, 3) and $2.7 \leq M_w \leq 5.0$ focal mechanisms (see. Sect. 3.3 and Fig. 4), respectively. Key: nt = total number of data (e.g., plane/slickenline); n = inverted data; σ1, σ2, σ3 = principal stress axes; Φ = stress ratio = (σ2-σ3)/(σ1-σ3). QR = quality ranking: AQRw as in Sperner et al. (2003) and A-QRfm as in Heidbach et al. (2010).

https://doi.org/10.5194/se-2021-76
Preprint. Discussion started: 11 June 2021


Solid Earth Discussions

3.3 Hypocenter location

To better characterize the 3D features of the structures lying in the region of the Mercure-Pollino sequence and to frame it in the geological scenario of the Calabrian-Lucanian border, we performed a high-quality hypocenter location. In previous works by Totaro et al. (2013 and 2015) and Brozzetti et al. (2017a), focused on the Mercure-Pollino sequence, the seismicity occurred in the time period 2010-2014 was analyzed. This allowed the authors to well characterize the seismic activity and to provide preliminary interpretations for geological features of the study area.

In this study, we sensibly enlarged the time window for earthquake analyses, with the data for all the earthquakes that occurred in the area between January 2010 and October 2018 (local magnitude greater than 1.0 and hypocentral depth range 0-30 km) collected from the Istituto Nazionale di Geofisica e Vulcanologia (INGV) Bulletin and the University of Calabria database. Automatic and manually revised P- and S-wave arrival time picks have been selected for this dataset. The recording network, including both temporary and permanent stations managed by the University of Calabria and INGV (D'Alessandro et al., 2013; Margheriti et al., 2013), consisted of 61 stations with a maximum epicentral distance of 150 km (Supplementary Fig. 1). We computed accurate absolute hypocenter locations by applying first the non-linear Bayloc earthquake location algorithm (Presti et al., 2004, 2008) and subsequently the double-difference relative location method HypoDD (v.2; Waldhauser, 2001), and using the 3D P-wave velocity model by Orecchio et al. (2011). The Bayloc algorithm gives for each earthquake a probability density cloud with shape and size related to the main factors involved in the location process (e.g., network geometry, picking errors), and allows a generally more accurate estimate of hypocenter parameters and location uncertainties with respect to the more commonly used linearized location methods (see e.g., Lomax et al., 2000; Husen and Smith, 2004; Presti et al., 2008). The application of the Bayloc algorithm to the collected dataset provided, on average, horizontal and vertical errors of the order of 1.0 and 1.5 km, respectively, and allowed us to obtain a well-constrained database that has been used as starting point for the subsequent analyses. As the second step, we applied the HypoDD algorithm, which minimizes phase delay-time residuals between pairs of events recorded at common stations (Waldhauser and Ellsworth, 2000). We computed the delay times from each event to its 30 nearest neighbors within 10 km distance, and to further ensure the robustness of the double-difference inversion. Only event pairs with at least eight phases observed at common stations were used. The final relocated dataset consists of 3109 events (Fig. 4 and Supplementary Fig. 1).

Before the 2010-2014 Pollino sequence, the instrumental data available within a range of nearly 75 km from the Mercure basin, referred to background seismic activity (Frepoli et al., 2005; Castello et al., 2006; Brozzetti et al, 2009). In this framework, the only phases of significant seismic activity which affected the region, were the above mentioned 2010-2014 Pollino sequence (Fig. 4 and Supplementary Fig. 1) and the moderate magnitude 1998-1999 Mercure seismic sequence that developed in the northern part of the homonym Quaternary basin (Guerra et al., 2005; Arrigo et al., 2005; Brozzetti et al., 2009). It started on September 1998 and lasted several months, showing some similarities to the recent Mercure-Pollino sequence (e.g., prevalent kinematics of focal mechanisms and hypocentral depth range). We explored the data available for this seismic sequence in order to compute a high-quality earthquake location, following the procedure already described for the 2010-2018 seismic

https://doi.org/10.5194/se-2021-76
Preprint. Discussion started: 11 June 2021

activity. Since the recording network operating during the 1998-1999 seismic phase was significantly different from today in terms of number of stations deployed in the region and their spatial distribution, the available data do not allow to reach the high level of constrain needed to perform the 3D structural model reconstruction.

3.4 3D Model building

The 3D Fault Model (3DFM) of the potentially seismogenic structures involved in the Pollino earthquakes was performed integrating the detailed Quaternary fault pattern provided in Brozzetti et al. (2009, 2017a) and integrated with new constrains from this paper, with the high-quality 2010-2018 seismicity dataset.
We applied the methodology defined by the Community Fault Model of Southern California (Nicholson et al., 2014; Nicholson et al., 2015; Plesch et al., 2014) which was also used, in previous works, to depict the subsurface geometry of the faults reactivated during recent Italian earthquakes (Lavecchia et al., 2017; Castaldo et al., 2018; Bello et al., 2021a).
In the present work, the uncertainties in identifying the active fault segments and determining the fault-earthquake associations were overcome thanks to the recent work of Brozzetti et al. (2017a) who discussed these aspects but without investigating the subsurface geometries of the sources.
We obtained the latter by interpreting as seismogenic fault-zone, the well-confined deformation volumes illuminated by the clustering of the hypocenters and using, for the 3D reconstruction, the Move suite software v. 2019.1 (Petroleum Experts Ltd). We describe in detail the steps of the 3D model building of the seismogenic sources in the following sections.

4 Results

4.1 Geological and Seismological Stress Tensors

The computed geological stress tensor (Fig. 5) shows a relevant percentage of fault/slip vector pairs (~53%) consistent with a uniform extensional stress field which is characterized by a N244 trending- and sub-horizontal σ3. The stress ratio Φ=0.22±0.13 and the rank quality is QRw=A (ranking as in Sperner et al., 2003). Nearly all the kinematic axes related to the inverted data belong to a normal-fault regime according to the triangle classification in Frohlich (2001) (see Fig. 5a).
It is worth noticing as 76% of the successfully inverted fault/slip vector pairs are related to the active fault planes belonging to the E- and W-dipping domains (Fig. 5a) while the remaining 24% include data related to the S-dipping system (CVN and POL). The latter evidence is consistent with the prevalent activation in the Late Quaternary of the E- and W-dipping fault systems.
The seismological stress tensor (Fig. 5b) obtained from inverting 50 actual fault planes (nt = 124 nodal planes), shows a normal fault regime with an ENE-WSW trending and sub-horizontal σ3 (N062/01 ±19). The stress ratio Φ=0.52 ±0.3 and the rank

https://doi.org/10.5194/se-2021-76
Preprint. Discussion started: 11 June 2021

quality is QRfm=A (ranking as in Heidbach et al., 2010). Most of the nodal planes show normal-fault kinematics (see the triangle diagram on the lower right corner of Fig. 5b).

Finally, in both the inversions, a normal-fault regime with sub-horizontal and collinear (~SW-NE trending) σ3-axis has been obtained. This result confirms the coherence between the geological and the present-day stress field and the persistence of this extensional regime since the Middle Pleistocene.

4.2 Time-space evolution of the Pollino sequence

The 2010-2018 seismic activity interval in the Pollino-Mercure area followed a peculiar evolution over time schematized in Fig. 3a-d. The distribution of epicenters concentrated in a series of neighboring clusters which were numbered as Cluster 0, 1, 2, and 3, from west to east, also according to their activation time. Such clusters, independent and unconnected, to each other, can be related to fault segments that are not in an along-strike continuity.

Cluster 0 includes the earliest (30/01/2010 - 31/07/2011), low magnitude ($1.0 \leq M_L \leq 2.9$) activity located in an NNE-SSW lengthened sector at the western boundary of the epicentral area. It is delimited westward by the more external segment of the E-dipping CRFS. In terms of generated events, this cluster was rather intermittent with periods characterized by moderate activity (Figs. 4a,c) alternating to substantially inactive ones (Figs. 4b,d). No significant seismicity occurred here during the 2015-2018 time span.

Cluster 1 was active after 05/10/2011 and during the entire 2010-2014 seismic sequence. It extended continuously, either northward and southward, reaching an NW-SE length of ~12 km (Fig. 4a-c). It comprehends the higher number of earthquakes and is largely the major cluster as regards the wideness (~60 km^2) and energy release. It includes 30 events with $M_L \geq 3.0$ besides the 25 October 2012 strongest event of the whole Pollino seismic activity. During the 2015-2018 interval, Cluster 1 area was affected by low seismic activity, mostly distributed in its northern and southern portions; conversely, its central part, where epicenters were particularly dense between 2011 and 2014, became nearly silent.

Overall, the surface extent of Cluster 1, which partly overlaps with Cluster 0, is limited eastward by the W-dipping RSB and VCT faults. Its southern boundary nearly coincides with the southeastern continuation of the AVN fault (PAC, Fig. 4c).

Cluster 2 was activated in May 2012 in the sector between the two WSW-dipping RSB and the MPR faults. It elongates in N-S direction, for ~7 km to the northwest of the Morano Calabro town. Afterward, it was nearly continuously active, particularly during the periods May-October 2012 and June-October 2014 (Fig. 4b,c); also in the period 2015-2018, significant seismicity persisted (Fig. 4d). Cluster 2 includes mainly low-magnitude events besides the strongest ones of 28 May 2012 and 6 June 2014 and three other earthquakes with $3.0 \leq M_L \leq 3.5$.

Further east, in the sector comprised between MPR and the alignment VPP-SDD-CAS faults, a minor seismicity cluster (Cluster 3) develop since December 2011 (Fig. 4a). Since then (2011-2018) it was affected by poor and low-magnitude seismicity, which however was clearly above the threshold of background seismicity, with two M_L=3.0 events (Fig. 4a-d).

https://doi.org/10.5194/se-2021-76
Preprint. Discussion started: 11 June 2021


Solid Earth Discussions

399 **4.3 3D Fault Model building**

400

401 Following the approach adopted and described in literature for the 3D fault model building (Lavecchia et al., 2017; Castaldo
402 et al., 2018; Bello et al., 2021a), we created several sets of closely spaced transects (half-width=2 km) to cross and sample
403 the seismogenic fault zones in different directions (Fig. 6). The first two sets (oriented SW-NE and NW-SE) are respectively
404 ~orthogonal (e.g., sections 1, 2 in Fig. 6) and ~sub-parallel (e.g., sections 3-6 in Fig. 6) to the ROCS (VCT and RSB), and
405 MPR active fault. A further NNE-SSW-striking set of transects was traced ~orthogonal to the active fault alignment bounding
406 eastward the area affected by the 2010-2014 seismic sequence, which includes the CPST and VPP faults (sections 7 and 8 in
407 Fig. 6).
408 The 3DFM building was carried out following three steps graphically depicted in Fig. 6 and synthetically described below.
409 *Step 1-Extrusion of fault traces to shallow depth*
410 The traces of the Quaternary faults, belonging to both E- ad W-dipping sets (Fig. 7) are "extruded" (i.e., projected
411 downward three-dimensionally) along-dip to reconstruct the so called "fault ribbons" (Fig. 7a). These latter are
412 extrapolated to a pre-set depth of 2 km b.s.l, according to the dip-angle of the fault planes measured at the surface during
413 fieldwork campaigns both of this work and from previous literature (Brozzetti et al., 2009, 2017a). In the absence of
414 these data, we assumed a fixed 60° dip-angle. The obtained ribbons are rimmed upward by the topographic surface
415 represented as a 10 m-resolution DEM (Tarquini et al., 2012). In the model, they close at the fault tip and their relationships
416 with the neighboring ribbons depend on the geometry of the transfer zone between adjoining faults.
417 *Step 2- Down-dip extrapolation of the faults along seismological sections*:
418 Starting from the analysis of the seismological transects (Fig. 6), the fault extrapolation at depth is based on the assumption
419 that the seismogenic volumes, (i.e., the main clusters of hypocenters), illuminate the portion of the activated fault zones.
420 In particular, the depth geometries were traced by connecting the surface "ribbons" (step 1) with the zones at depth where
421 seismicity is more dense (i.e., where the concentration of hypocenters is higher; Fig. 7b,c) downward to the base of the
422 seismogenic layer. The latter, according to the model proposed in Brozzetti et al. (2017a), corresponds to an E-dipping
423 basal detachment.
424 We also considered the attitudes of the preferential fault planes from focal mechanisms falling within each section. In
425 general, this step is relatively simple in those cases where seismicity originates on fault zones having regular shape,
426 whereas it gets complicated in areas, as the study one, where multiple faults, characterized by sharp strike-changes,
427 interact. In such cases, seismicity distributes in geometrically complex volumes and the hypocentre clusters have irregular
428 contours, possibly because include groups of events generated on adjacent faults.
429 *Step3- Building of 3D fault surfaces through Delaunay triangulation method*
430 This method automatically allows reaching the final 3D reconstruction of the seismogenic faults (Fig. 7c,d) by
431 interpolating all the elements derived by the previous two steps.
432 After joining at depth the fault ribbons with the subsurface sources, we obtained the seismogenic patches by projecting

https://doi.org/10.5194/se-2021-76
Preprint. Discussion started: 11 June 2021

433 on each reconstructed fault plane the seismicity cluster as density contour (Fig. 6d). This depiction allows visualizing,
434 with a good degree of approximation, the portion of the fault which released most of the seismicity during the considered
435 time interval.
436 This methodology made it possible to refer with good confidence the hypocentral distribution of the 2010-2018 seismicity
437 to the causative faults confirming that Cluster 1 and Cluster 2 well-correlate respectively with the SW-dipping ROCS
438 (RSB+VCT) and MPR faults. The westernmost concentration of hypocentres (i.,e., Cluster 0), given its location, may be
439 due either to the deeper portion of the VCT fault or to the E-dipping AVN Fault, which act as the lower boundary of the
440 W-dipping fault set (Fig. 7c,d).
441

https://doi.org/10.5194/se-2021-76
Preprint. Discussion started: 11 June 2021

Solid Earth
Discussions
Open Access
EGU

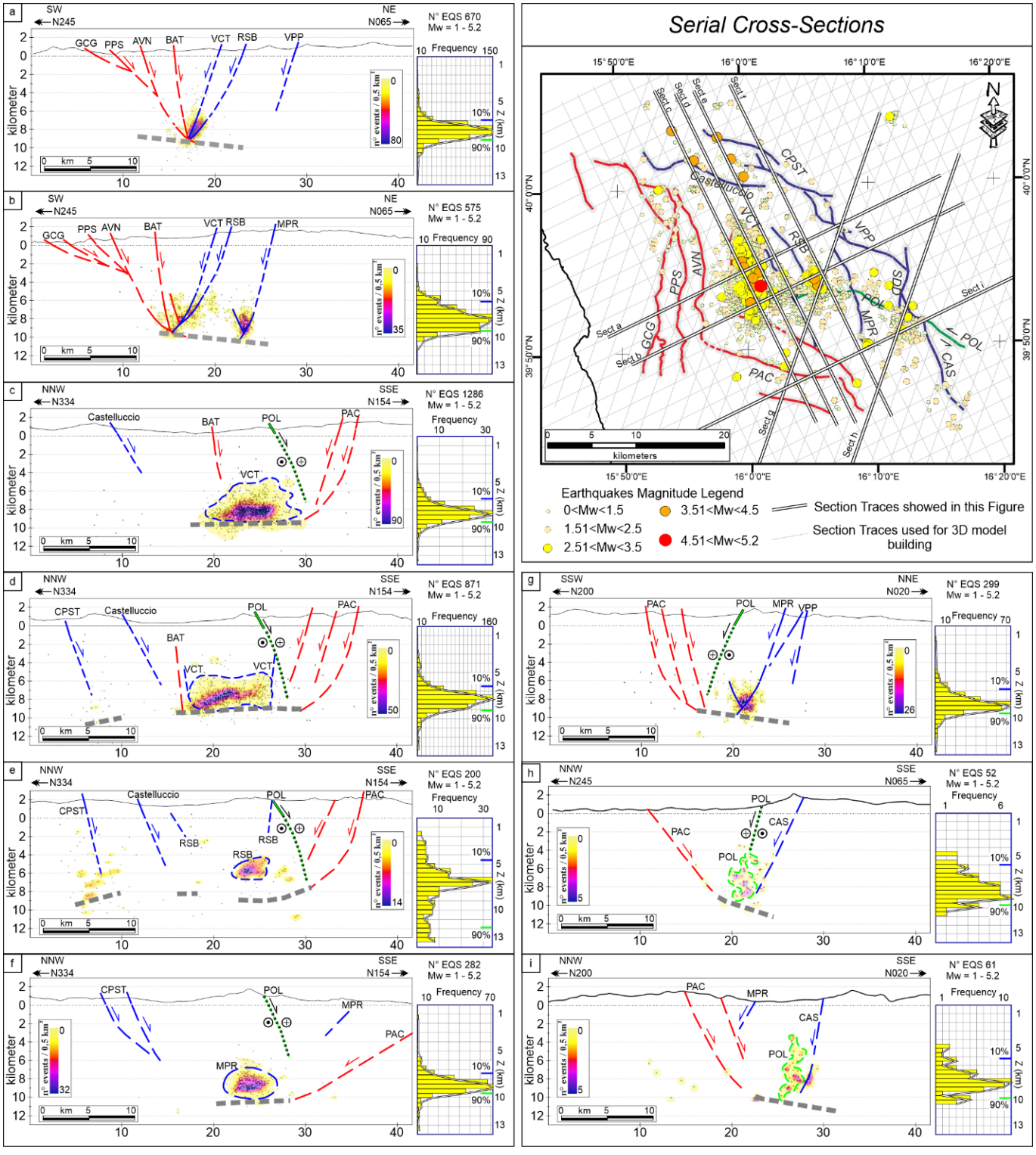

https://doi.org/10.5194/se-2021-76
Preprint. Discussion started: 11 June 2021

Solid Earth
Discussions
Open Access
EGU

443 **Figure 6:** Epicentral (map – upper right) and hypocentral distributions (sections – a to i) of the 2010-2018 seismic activity
444 occurred in the Pollino area. In the vertical cross-sections the earthquakes have been reported also as density contours
445 computed using Kernel Density Estimation. The histograms close to each section show the depth distribution of the sequence.
446 The traces of the overall dataset of serial cross-sections analysed in this study are reported in map view as thin grey lines while
447 the bold lines relate to the sections shown in this figure.
448

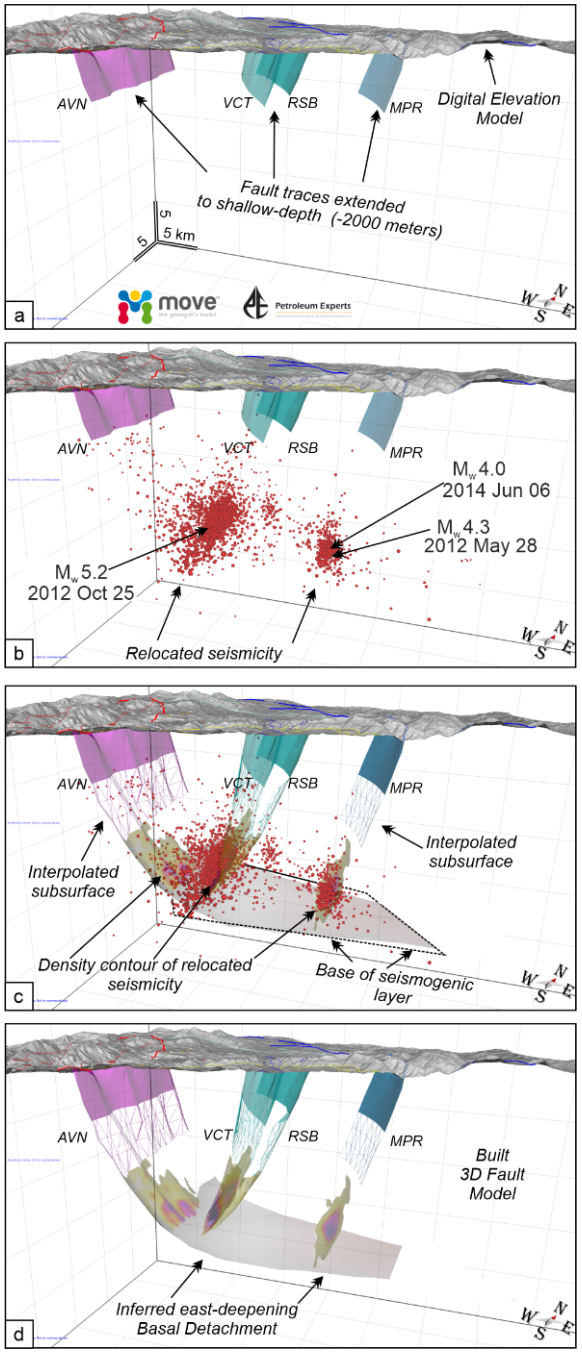

449

https://doi.org/10.5194/se-2021-76
Preprint. Discussion started: 11 June 2021

Figure 7: 3D fault model building, from surface (represented by a 10 m-resolution DEM – Tarquini et al., 2012) to the base of the seismogenic layer. Faults acronyms as in Figure 2. (a) "Fault ribbons" obtained by extruding the fault traces mapped at surface up to shallow depth (2 km b.s.l.), and considering the fault dip-angles measured in the field. (b) 3D fault model as in (a) with relocated seismicity. (c) Fault extrapolation at (seismogenic) depth through the clusters of hypocenters. The modelled faults connect the ribbons with the zones at depth where concentrations of hypocenters is higher. The density contours of the seismicity and the base of the seismogenic layer are also shown (see also panel d). (d) Final 3D fault model obtained integrating the detailed Quaternary fault pattern with the high-quality 2010-2018 seismicity dataset.

4.4 3D Fault Model of the Pollino area Quaternary and active fault system

The 3DFM obtained to the depth of ~10-12 km (Fig. 8), as well as including the seismogenic fault system activated during and after the Pollino seismic sequence (i.e., 2010-2018), represented by CRFS, ROCS, and MPR, also encompasses those faults that, while showing no direct evidence of recent seismic activity, play a significant role in the seismotectonic frame of the area. In other words, we also considered the structures that border the reactivated faults, either beneath or laterally, representing possible barriers to the propagation of coseismic faulting.

We interpreted the westernmost fault structures (i.e., GCG and PPS) whose deep geometry is not strictly constrained by subsurface data, according to the structural extensional style proposed by Brozzetti et al. (2017a). This is coherent with the reconstructions of the active extensional belt of the southern and central Apennines described in the literature (Barchi et al., 2007; Amicucci et al., 2008; Brozzetti et al., 2011, 2017a, 2017b; Lavecchia et al., 2017).

Overall, this style is characterized by an asymmetric extension driven by a low-angle (20° to 35°) E-dipping detachment fault which represents the basal decollement of all the other extensional structures.

In the model, all the faults are traced at the surface with their outcrop dip-angle and evolve downward with nearly-listric geometries to join the detachment at increasing depth from west to east. The latter represents, the structurally controlled base of the seismogenic layer.

We interpreted the GCG (Figs 1b, 8), which crops out at low-angle and overcomes all the other east-dipping faults in terms of slip and associate extension, as the currently inactive break-away zone of such a detachment.

The AVN and BAT (Figs 1b, 8), which are the easternmost E-dipping splays, are suggested to be active and seismogenic, being possibly the causative structures of the Cluster 0 of hypocenters recognized during the 2010-2014 activity (Fig. 4).

In such a model, also the W-SW-dipping ROCS and MPR faults, which we consider the main sources of the 2010-2014 seismic sequence, are downward confined by the E-dipping detachment (Fig. 8a,a1).

Further east, the 3DFM has been widened to include the W-dipping CPST and VPP faults, considered the outer seismogenic front of the extensional system (Brozzetti et al., 2009).

The yellow surface shown in Fig. 8c,d, depicts, in nearly frontal view, the 3D shape of the POL and its westernmost segment (CVN) bounding to the north of the Campotenese basin. The along-strike continuity of this fault is interrupted by the W-

https://doi.org/10.5194/se-2021-76
Preprint. Discussion started: 11 June 2021

dipping ROCS and MPR faults, coherently with the cross-cut relationships observed in the field (Fig. 1b).
In Fig. 8d, the depth geometry of POL and CVN interrupts the NNE-dipping AVN (violet surface in Fig. 8d) which acts as the southern and basal boundary of the entire active fault system.
Finally, the comparison between the reconstructed 3D-model and the plotted re-located seismicity evidently shows that almost the whole 2010-2018 hypocenters correlates with the W-dipping structures but without affecting their southern termination zones. In other words, no or very few events locate south of the intersection with POL and CVN faults.
This latter observation suggests that although the POL and CVN did not play an active role in the origin of the considered seismic activity, play a significant role in influencing its distribution.

https://doi.org/10.5194/se-2021-76
Preprint. Discussion started: 11 June 2021

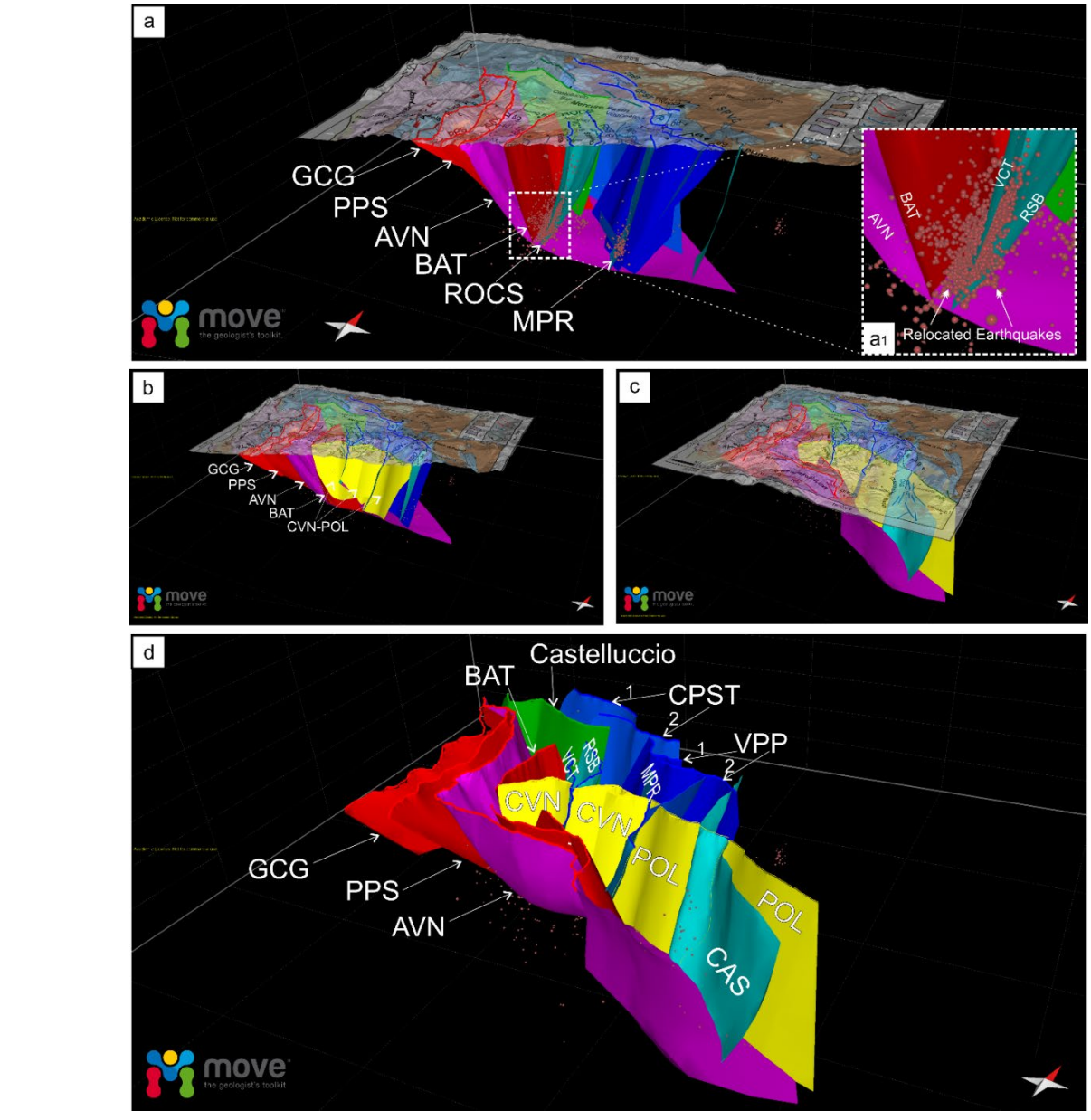

Figure 8: Tri-dimensional model of the extensional system at the Calabrian-Lucanian boundary extrapolated down to the depth of ~10-12 km. The geological-structural map used as a base over a 10 m-resolution DEM is from Brozzetti et al., 2017a. Fault surfaces are those belonging to the seismogenic fault system activated during and after the Pollino seismic sequence (2010-2018), and those playing a key role in the seismotectonic context of the area. The faults belonging to the E-NE-dipping CRFS fault set are represented in red and violet, whereas the antithetic ROCS and MPR faults are shown as blue surfaces (fault acronyms as in Figure 2). Yellow surface is the tri-dimensional surface of the POL and its westernmost segment (CVN) bounding, to the north, the Campotenese basin.

https://doi.org/10.5194/se-2021-76
Preprint. Discussion started: 11 June 2021

505 **5 Discussion**

506

507 **5.1 Maximum expected magnitude**

508

509 Coherently with what is observed in most of the Apennine chain, the upper crustal Pollino seismicity developed in response
510 to WSW- ENE oriented extension. This is well constrained by the focal solutions of the strongest events (M_w 5.2, 25 October
511 2012; M_w 4.3, 28 May 2012, and M_w 4.0, 6 June 2014 earthquakes) and all the $M_w \geq 3.5$ earthquakes that occurred during the
512 2010-2014 seismic sequence.
513 The tensor provided by the inversion of fault/slip data, collected on the Quaternary faults (Figs. 2, 3 and 5a), is also extensional
514 and nearly co-axial to the seismological one. Such consistency suggests that the present stress field is in continuity with the
515 long-term one, which is active at least since the Early-Middle Pleistocene as already suggested by previous works
516 (Papanikolaou and Roberts, 2007; Brozzetti et al. 2009; 2017a).
517 Comparing the distribution of the whole 2010-2018 seismic activity with the Late Quaternary structures mapped at the surface,
518 we maintain that the ROCS and the MPR faults are respectively suitable as the seismogenic sources for the Mormanno (2012,
519 M_w 5.2) and Morano Calabro (2012, M_w 4.3 and 2014, M_w 4.0) earthquakes.
520 However, our 3DFM goes beyond establishing the earthquake-structure associations and allows defining a strictly constrained
521 parameterization of the sources and assessing their seismogenic potential.
522 From the overall fault model of Fig. 9a (the same of Fig. 8 but in zenithal view) we extracted the plan view of the W-dipping
523 seismogenic faults (Fig. 9b). This representation depicts irregularly-shaped seismogenic boxes which are bordered to the east
524 by the fault traces and, on the opposite side, by the projection at the surface of the branch line of each fault from the base of
525 the seismogenic layer. Some of the aforementioned boxes include historical or instrumental earthquakes (colored squares in
526 Fig. 9b) while others are not associated with any significant event.
527 The performed 3D reconstruction allowed us precisely estimating the effective area extent of all the fault segments, despite
528 their irregular shape and complex segmentation pattern. The calculated areas (Fig. 9c left white column), inserted in the
529 appropriate scaling relationships, provide the maximum expected magnitude that each fault might release in the borderline
530 case in which the coseismic rupture affects its entire plane (Fig. 9c, yellow, blue, and brown columns).
531 The maximum magnitude values obtained using the regressions as a function of the surface fault length (Fig. 9c, right white
532 column) are listed in Fig. 9c (light-blue, green, and grey columns).
533 Finally, the two graphs of Figs. 9d (fault area-based scaling relationships) and 9e (fault length-based scaling relationships)
534 allow comparing the values determined, for all the investigated active normal faults, using six different empirical relations
535 (Wells and Coppersmith, 1994; Wesnousky, 2008; Leonard, 2010; Stirling et al., 2013).
536 It is evident that, for each fault, the maximum expected magnitude reported in Fig. 9d (computed using fault area) is lower
537 than that plotted in Fig. 9e (computed using fault length) and also the range of variation (length of yellow bars on Figs 9d and
538 9e graphs) is narrower for the values computed on the ground of fault-area regressions.

https://doi.org/10.5194/se-2021-76
Preprint. Discussion started: 11 June 2021

As the difference in the obtained results is significant, a matter of primary importance concerns which scale relationships are to be used for the evaluation of the maximum expected magnitudes.

In the light of our results, we suggest that, wherever possible, the selection must be made taking into account the 3D reconstructed geometry of the faults, which allows determining as precisely as possible its shape and parameters (Supplementary Table 1).

The extensional faults system of the Calabrian-Lucanian border is markedly asymmetrical (Brozzetti, 2011; Brozzetti et al., 2017a, 2017b). It is characterized by high-angle W-dipping active faults (ROCS, MPR, VPP, CPST and CAS, Fig. 8a-d) delimited downward by an E-dipping, low-angle, detachment fault (violet surface in Fig. 8a) from which the high-angle active splays (AVN and BAT, Figs. 7,8) branch upward.

The 3D reconstruction of the fault system highlights that the depth reached by the W-dipping faults, which strictly influence their areal extension, depends on their position within the hanging wall of the detachment. In other words, faults with comparable length at the surface may have significantly different areas, depending on the reached depths.

The CPST, VPP and CAS belong to the easternmost extensional alignment and crop out at great distance from the GCG break-away zone. Consequently, they intersect at the higher depth of the basal detachment and have the maximum area extent among the W-dipping fault set (Fig. 9a,d) implying, in turn, different values of the maximum expected magnitude.

From the previous reasoning, it follows that the 3DFM, which allows estimating accurately the subsurface extent and areas of the seismogenic faults, leads to prefer for the assessment of the associate seismogenic potential, the scaling relationships based on the fault area.

In our case, by applying this type of regressions to the W-dipping faults identified to be the sources of the 2010-2014 seismic sequence, we calculated the maximum expected magnitude of ~M_w=6.1 for the VCT and the RSB, and of ~M_w= 6.2 for the MPR. A value of ~ M_w=6.4 could be reached in the case of the complete and concurrent ruptures on both the ROCS segments (joined RSB+VCT).

It is noticeable that the aforesaid values are sensibly higher than the magnitudes of the earthquakes recorded to date in the Mercure-Campotenese area (Figs 1b, 9b) suggesting that the considered faults released only partially their seismogenic potential during historical times.

This inference also agrees with the distribution and evolution of the 2010-2018 seismic activity. The clusters of the relocated hypocenters concentrated in the deepest parts of the ROCS and MPR faults (Fig. 6) confirming that only a portion of such faults ruptured during the sequence, without the rupture reaching the surface.

https://doi.org/10.5194/se-2021-76
Preprint. Discussion started: 11 June 2021

Solid Earth
Discussions
Open Access
EGU

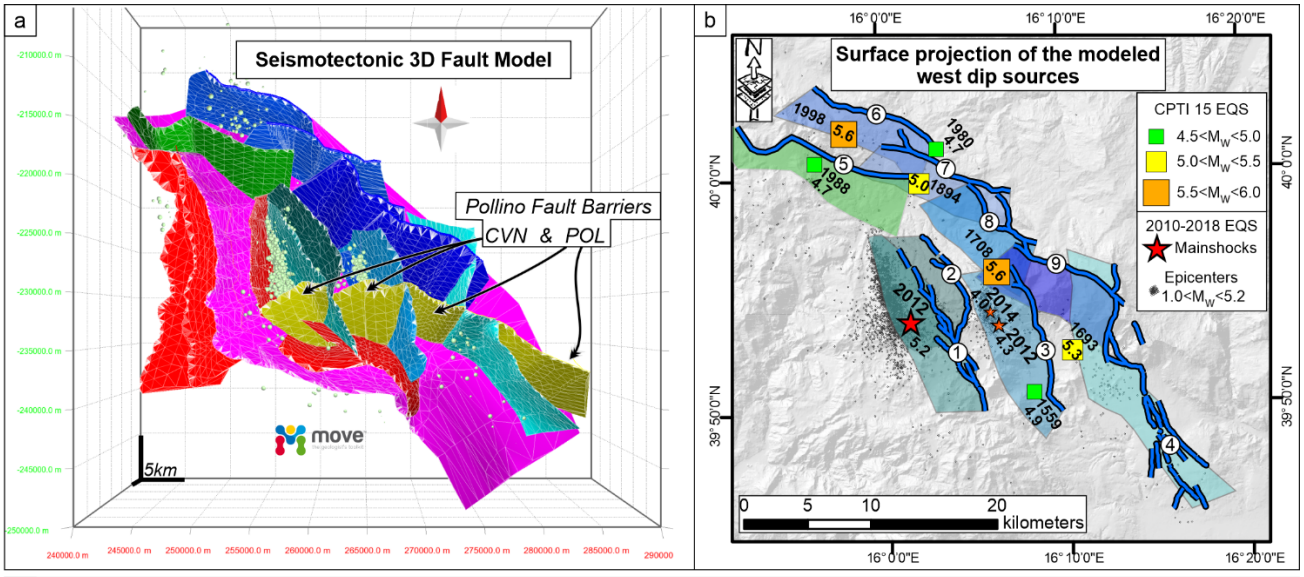

c

Scaling Relationships for Seismic-Hazard Analysis

Fault Acronym	Area km²	M_w(a)	M_w(b)	M_w(c)	Length km	M_w(d)	M_w(e)	M_w(f)
VCT (1)	131.07	6.1	6.2	6.1	15.16	6.5	6.7	6.8
RSB (2)	123.39	6.1	6.1	6.1	12.82	6.4	6.7	6.8
ROCS (RSB + VCT)	254.46	6.4	6.4	6.4	27.98	6.8	6.8	7.0
MPR (3)	153.01	6.2	6.2	6.2	13.33	6.4	6.7	6.8
CAS (4)	286.49	6.5	6.5	6.4	20.64	6.6	6.7	6.9
Castelluccio (5)	120.35	6.1	6.1	6.1	16.12	6.5	6.7	6.9
CPSTa (6)	164.35	6.2	6.2	6.2	11.04	6.3	6.6	6.7
CPSTb (7)	171.33	6.2	6.3	6.2	11.28	6.3	6.6	6.7
CPST a+b	335.68	6.5	6.6	6.5	22.32	6.6	6.8	7.0
VPPa (8)	150.06	6.2	6.2	6.2	8.00	6.1	6.5	6.6
VPPb (9)	129.28	6.1	6.1	6.1	9.49	6.2	6.6	6.7
VPP a+b	279.34	6.5	6.5	6.4	17.50	6.5	6.7	6.9
SPVC (VPP+CPST)	615.02	6.8	6.8	6.8	39.81	6.9	6.9	7.2

a Leonard 2010 (Area), dip slip
$M_w = 4.00 + \log A$

b Wells & Coppersmith 1994 (Area), all slip
$M_w = 4.07 + 0.98 \log A$

c Wells & Copp. 1994 (Area), normal slip
$M_w = 3.93 + 1.02 \log A$

d Wells & Copp. 1994 (Length), normal slip
$M_w = 5.08 + 1.16 \log L$

e Wesnousky 2008 (Length), normal slip
$M_w = 6.12 + 0.47 \log L$

f Stirling et. al. 2013 (Length), normal slip
$M_w = 5.88 + 0.88 \log L$

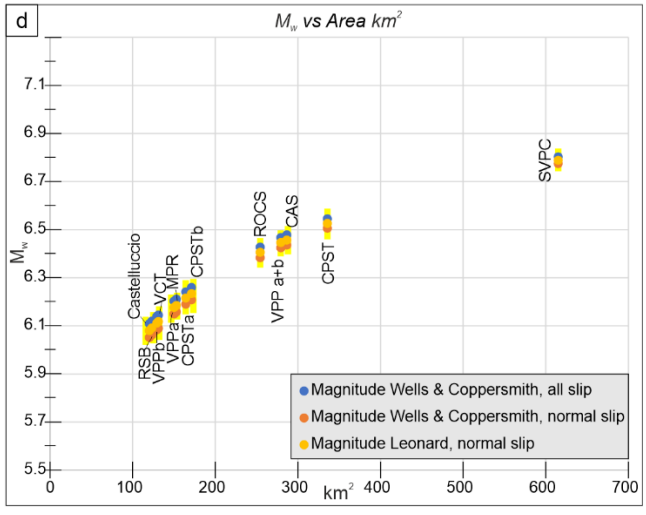

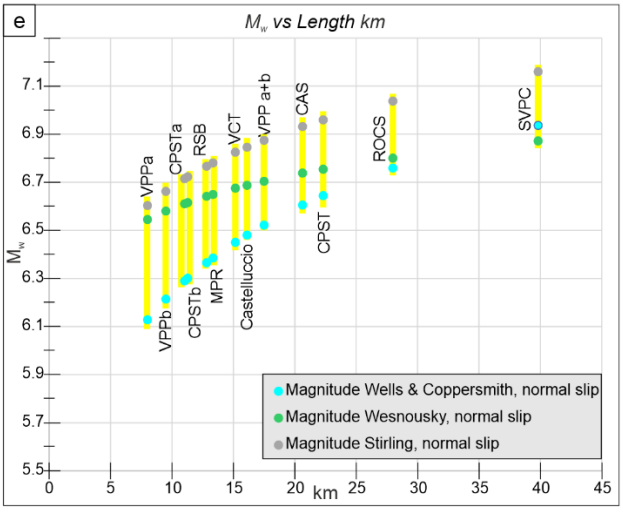

568

https://doi.org/10.5194/se-2021-76
Preprint. Discussion started: 11 June 2021

569 **Figure 9:** (a) Seismotectonic 3D Fault Model in map view. (b) Box representation of the 3D seismotectonic model of the
570 West-dipping seismogenic faults in its detailed segmentation pattern. The associated historical earthquakes from CPTI15 v3.0
571 ($4.5<M_w<6.0$; Rovida et al., 2020, 2021) and the epicentral distribution of the 2010-2018 seismic activity occurred in the
572 Pollino area ($1.0<M_w<5.2$) are also reported. (c) Maximum expected magnitude according to scaling laws (Wells &
573 Coppersmith 1994, Wesnousky 2008, Leonard 2010, Stirling et al. 2013) and calculated based on area (A) and length (L) of
574 each fault. (d) Graph showing fault- area based scaling relationships. (e) Fault length-based scaling relationships comparing
575 the values determined for all the investigated active normal faults and using six different empirical relations reported in panel
576 (c).
577
578
579 **5.2 Seismogenic patches activated during 2010-2014 seismic sequence**
580
581 An attempt to reconstruct the seismogenic patches activated on the ROCS and MPR faults during 2010-2014 seismic sequence,
582 is shown in Fig. 10. The patches can be considered the reasonable approximation of the actual portion of the faults which broke
583 during the mainshock and the sequence of the early aftershocks.
584 Operationally, we obtained the boundaries of the patches by projecting the relocated hypocenters on the reconstructed fault
585 surface and depicting their distribution using the Kernel density geostatistical analyst, available as a tool of the ESRI ArcGIS
586 software package.
587 At the depth at which the hypocenters of the 2010-2014 seismicity concentrate, the two segments of the W-dipping ROCS
588 fault set, can be considered joined to form a single structure, thus a unique seismogenic patch was reconstructed.
589 The temporal analysis of the sequence, showed that their overall extent was already well defined within the first 72 hours after
590 the major events. Anyhow, inside the surrounding volumes, some seismicity had started before the mainshock and also
591 continued to persist constantly throughout the development of the entire sequence so that they include a percentage ≥ of 70%
592 of the whole hypocenters locations.
593 The delimitation of each seismogenic patch and its subsequent parameterization allowed us to verify if there is a direct
594 correlation between its dimensions and the magnitude released by each fault during the mainshocks.
595 The patches obtained over the VCT and MPR fault surfaces correspond to the violet contoured area shown in Fig. 10. Their
596 along-strike elongation and area extent can be assumed respectively as the effective Subsurface Rupture Length and Rupture
597 Area (RLD and RA in Fig. 10b, and 10c, respectively, according to Wells and Coppersmith, 1994) associated with the M_w 5.2
598 Mormanno (on VCT fault) and M_w 4.0 and 4.3 Morano Calabro (on MPR fault) earthquakes.
599 The parameters obtained for the VCT fault are RLD= 4.9 km and RA= 8.3 km^2. The values of RLD= 1.2 km and RA= 3.6 km^2
600 are assessed for the MPR fault.
601 Introducing the aforesaid parameters in the appropriate scale relationships (Fig. 10b,c) we observe a good agreement, or a
602 slight overestimation, between the theoretical magnitudes based on the Subsurface Rupture Length and the magnitudes of the
603 mainshocks. The values obtained for the VCT fault (causative of the M_w 5.2 Mormanno earthquake) are = M_w 5.3 whereas for
604 the MPR fault (causative of the M_w 4.0 and 4.3 Morano Calabro earthquakes) is M_w=4.5.

https://doi.org/10.5194/se-2021-76
Preprint. Discussion started: 11 June 2021

605 The magnitude calculated using the RA-based relationships provides values slightly lower than expected for the VCT
606 ($4.9<M_w<5.0$) and little higher for the MPR ($4.5<M_w<4.6$).
607 In both cases, however, the magnitude values obtained using the scale relationships differ from those observed by an amount
608 <0.3.
609

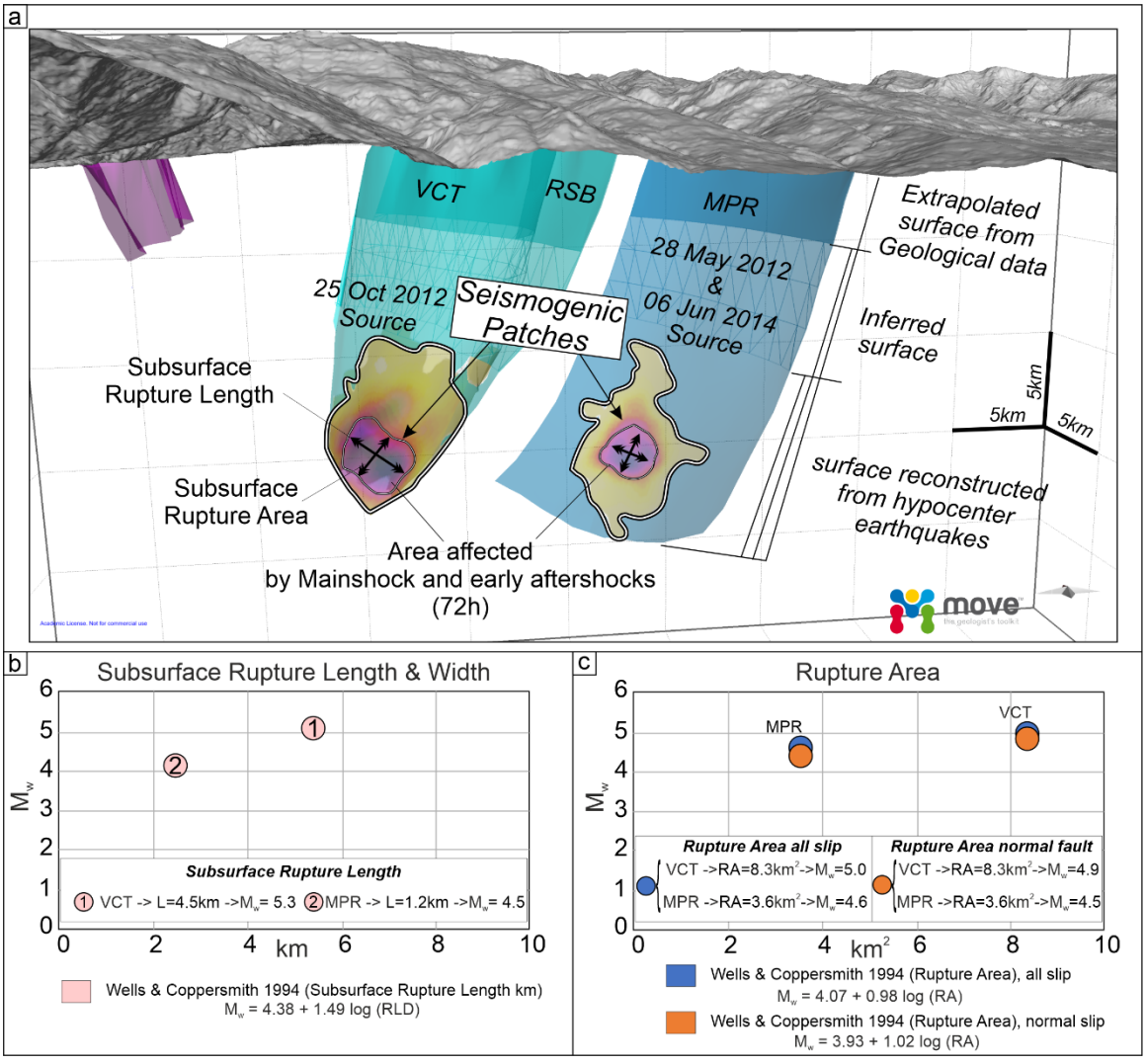

610
611

612 **Figure 10:** (a) Seismogenic patches activated during the 2010-2014 seismic sequence on VCT and MPR faults. The along-
613 strike elongation and area extent, shown by black arrows, are assumed to be the effective subsurface rupture length and rupture
614 area (RLD and RA, according to Wells and Coppersmith, 1994) associated with the M_w 5.2 Mormanno (on VCT fault) and
615 M_w 4.0 and 4.3 Morano Calabro (on MPR fault) earthquakes, respectively. (b) and (c) show the RLD and RA, respectively,
616 obtained for both the VCT and MPR faults. A comparison between the theoretical magnitudes (obtainable with scale
617 relationships) based on the subsurface rupture length and the magnitudes of the mainshocks are also shown.

https://doi.org/10.5194/se-2021-76
Preprint. Discussion started: 11 June 2021

618 **5.3 Possible geometric restraints to coseismic rupture propagation**
619
620 The high-precision seismological dataset we used, demonstrates that the two main clusters of earthquakes of the 2010-2018
621 seismicity were generated by as many independent sources related to the sub-parallel, 10 to 15 km-long, ROCS and MPR
622 faults.
623 Brozzetti et al. (2017a) highlighted that the above seismogenic style, characterized by a perpendicular-to-fault strike evolution
624 of the seismic activity, is unlike from those which followed the major instrumental earthquakes recorded in the Apennine
625 Extensional Belt of Italy in recent years, such as the Colfiorito 1997 (M_w 6.0), L'Aquila 2009 (M_w 6.3) and Norcia 2016 (M_w
626 6.5) events (Chiaraluce et al. 2011, 2017; Lavecchia e al., 2011, 2012, 2016). They also speculated that this peculiar behavior
627 of the 2010-2014 Pollino seismic sequence could have been controlled by the geometric fault pattern of the area, which is
628 characterized by WSW-dipping seismogenic faults bounded southward by nearly E-W pre-existing structures. These latter
629 which are genetically related to the regional-scale, long-lived, "Pollino lineament" *s.l.*" (Bousquet, 1969, 1971; Ghisetti and
630 Vezzani, 1982, 1983; Knott and Turco, 1991; Van Dijk et al., 2000) determine the abrupt contact between the Apennine
631 carbonate platform unit and the San Donato metamorphic core complex (Grandjaquet 1962; Servizio Geologico Nazionale,
632 1970; Amodio Morelli 1976). The cross-cut relationships detected in the field between the ROCS-MPR set and POL-CVN,
633 highlighted in our 3D model (Fig. 8d), lead us to exclude the latter fault to have a present seismogenic role, as also supported
634 by the distribution of the instrumental earthquakes which clusterized along with N-S-striking crustal volumes.
635 However, it cannot be excluded that this significant geological boundary exerts an influence on the southward propagation of
636 the presently active seismogenic faults, driving the eastward transfer of the active extensional deformation belt. This inference
637 is confirmed by the spatial distribution of the hypocentres of the whole 2010-2018 relocated seismicity which, with sporadic
638 exceptions, is confined within the CVN footwall (Fig. 8d).
639
640 **6 Conclusions**
641
642 We reconstructed in detail the 3D geometry and kinematics of the interconnected fault pattern responsible for the moderate-
643 magnitude earthquakes which recently affected the Pollino area.
644 The main original outcomes that we have achieved are summarized as follows:
645 - We computed the geological and seismological stress tensor and demonstrate that they are consistent with a uniform normal
646 faulting regime characterized by an ENE-WSW trending, sub-horizontal σ3. This result confirms the coherence between the
647 long-term and the present-day stress field and the persistence of this extensional regime at least since the Middle Pleistocene.
648
649 - The 2010-2018 seismic activity which affected the study area followed a peculiar evolution over time characterized by
650 concentration of epicenters in a series of sub-parallel ~NNW-SSE elongated clusters, independent and unconnected, which

https://doi.org/10.5194/se-2021-76
Preprint. Discussion started: 11 June 2021

651 can be related to two major near coaxial WSW-dipping faults possibly splaying from a common east-dipping basal detachment
652 and almost concurrently releasing seismicity.
653
654 -The accurate hypocenter re-locations, obtained by applying the non-linear Bayloc earthquake location algorithm, followed by
655 the double-difference relative location method HypoDD, and using a 3D P-wave velocity model, provided a high-resolution
656 seismological dataset. The latter was found to be of excellent quality for the purposes of 3D modelling. The correlation between
657 the geometry of the active faults at the surface, and the distribution of seismicity at depth, allowed us to reconstruct the 3D
658 geometry of the seismogenic sources which released the 2010-2018 seismicity. This reconstruction was the interpretative key
659 to obtain the overall model of the Quaternary and active fault system of the northern Calabria-Lucania Apennines, extrapolated
660 down to the depth of ~10-12 km. The model includes all the faults playing a significant role, either direct or indirect, on the
661 seismogenesis of the study area.
662
663 -Based on the dimension and shape of the seismogenic patches, an estimate of the maximum expected magnitudes has been
664 calculated using appropriate scaling relationships, for all the active faults of the Pollino area. The complete rupture of
665 individual W-dipping faults which are recognized to have been causative of the 2010-2014 seismic sequence are expected to
666 release a magnitude of ~M_w= 6.1 for the VCT and the RSB, and of ~M_w= 6.2 for the MPR. Higher values, up to M_w=6.4,
667 could be reached in the case of the complete and concurrent rupture on both RSB and VCT. The obtained values exceed the
668 magnitudes of the associate earthquakes which struck the area to date, implying that the aforesaid faults released only partially
669 their seismogenic potential.
670
671 - The delimitation of the fault patches broken during the 2010-2014 seismic sequence, and their geometrical parameterization,
672 allowed us to verify that a high consistency occurs between the theoretical magnitudes based on the Subsurface Rupture Length
673 and the magnitudes of the mainshocks.
674 The estimates provided, for the VCT fault (which released the M_w 5.2 Mormanno earthquake) a M_w 5.3 and, for the MPR fault
675 (which released the M_w 4.0 and 4.3 Morano Calabro earthquakes), a M_w=4.5. The magnitudes calculated using the relationships
676 based on the Subsurface Rupture Area ($4.9<M_w<5.0$ for the VCT and $4.5<M_w<4.6$ for the MPR), instead deviate more from
677 the observed values.
678
679 - Our reconstruction confirms that the western segment of the Pollino Fault, despite not being presently active, seems to
680 maintain a significant seismotectonic role. In fact, juxtaposing crustal sectors with different structure and composition
681 (Apennine platform domain to the north, and San Donato metamorphic core to the south) acts as a barrier to the southern
682 propagation of the seismogenic faults of the Mercure-Campotenese sector (ROCS, MPR), limiting their dimensions and
683 seismogenic potential.
684

https://doi.org/10.5194/se-2021-76
Preprint. Discussion started: 11 June 2021

In conclusion, we want to point out that also in the case of moderate-to-minor seismic sequences, as the Pollino 2010-2014 one, the approach based on the three-dimensional reconstruction of the directly involved, as well as neighboring, Quaternary fault surfaces, represents a real breakthrough in the seismotectonic analysis and, ultimately, in the cognitive path that leads to a better assessment of the seismic hazard of an active area.

Author contribution:

DC, FB conceived and conducted the study. FB, DC, FF, SB Wrote the manuscript. DC developed the 3D model. DC, SB, FF did GIS analysis and mapping. DC, FB, SB performed the fieldwork. CT, DP, BO, RdN, led the seismological analysis. CT, DP, BO, processed seismological data. FF did geological and seismological stress field inversion. DC prepared the figures. GL, SB, FB reviewed the figures. DC, SB prepared the GIS geological database. All authors reviewed the final version of the manuscript.

Competing interests: The authors declare no conflict of interest.

Acknowledgements:

Funding was from the DPC-INGV PROJECTS-S1 2014-2015 URUnich, resp. F. Brozzetti and from DiSPUTer Department research funds to G. Lavecchia and F. Brozzetti. This research was supported by PRIN 2017 (2017KT2MKE) funds from the Italian Ministry of Education, University and Research (P.I. Giusy Lavecchia). The author is grateful to Petroleum Experts, who provided them with the Move, 2019.1 suite software licence.

References

Allmendinger, R. W., Cardozo, N., and Fisher, D.: Structural geology algorithms: Vectors and tensors in structural geology: Cambridge University Press (book to be published in early 2012) 2012.

Amicucci, L., Barchi, M.R., Montone, P., and Rubilani, N.: The Vallo di Diano and Auletta extensional basins in the southern Apennines (Italy): a simple model for a complex setting, Terra Nova, 20, 475-482, https://doi.org/10.1111/j.1365-3121.2008.00841.x, 2008.

Amodio Morelli, L., Bonardi, G., Colonna, V., Dietrich, D., Giunta, G., Ippolito, F., Liguori, V., Lorenzoni, S., Paglionico, A., Perrone, V., Piccarreta, G., Russo, M., Scandone, P., Zanettin-Lorenzoni, E., and Zuppetta, A.: L'Arco calabro peloritano nell'orogene appenninico-maghrebide, Mem. Soc. Geol. It. 17, 1-60, 1976.

https://doi.org/10.5194/se-2021-76
Preprint. Discussion started: 11 June 2021

718 Angelier, J., and Mechler, P.: Sur une méthode graphique de recherche des contraintes principales également utilisable en
719 tectonique et en séismologie: la méthode des dièdres droits, B. Soc. Gèol. Fr., 7, 1309–1318, 1977.
720
721 Arrigo, G., Roumelioti, Z., Benetatos, C., Kiratzi, A., Bottari, A., Neri, G., Termini, D., Gorini, A., and Marcucci, S.: A source
722 study of the 9 September 1998 (Mw 5.6) Castelluccio Earthquakes in Southern Italy using Teleseismic and strong motion data,
723 Nat. Hazards 00, 1-16, doi:10.1007/s1001 1069-1005-4644-1001, 2005.
724
725 Ascione, A., Mazzoli, S., Petrosino, P., and Valente, E.: A decoupled kinematic model for active normal faults: insights from
726 the 1980, MS=6.9 Irpinia earthquake, southern Italy, GSA Bull 125, 1239-1259, doi:10.1130/B30814.1, 2013.
727
728 Barchi, M. R., De Feyter, A., Magnani, M. B., Minelli, G., Pialli, G., and Sotera, B. M.: Extensional tectonics in the northern
729 Apennines (Italy): Evidence from the CROP03 deep seismic reflection line, Mem. Soc. Geol. Ital., 52, 527– 538, 1998.
730
731 Barchi, M., Lavecchia, G., Galadini, F., Messina, P., Michetti, A. M., Peruzza, L., Pizzi, A., Tondi, E., and Vittori, E.: Sintesi
732 delle conoscenze geologiche sulle faglie responsabili dei terremoti maggiori in Italia Centrale: Parametrizzazione ai fini della
733 caratterizzazione della pericolosità sismica, Gruppo Naz. per la Difesa dai Terremoti, CNR, Rome, 1999.
734
735 Barchi, M., Amato, A., Cippitelli, G., Merlini, S., and Montone, P.: Extensional tectonics and seismicity in the axial zone of
736 the southern Apennines, Boll. Soc. Geol. It. (Ital. J. Geosci.) 7, 47-56, 2007.
737
738 Bello S., de Nardis R., Scarpa R., Brozzetti F., Cirillo D., Ferrarini F., di Lieto B., Arrowsmith R. J., and Lavecchia G.: Fault
739 Pattern and Seismotectonic Style of the Campania-Lucania 1980 Earthquake (Mw 6.9, Southern Italy): New Multidisciplinary
740 Constraints, Frontiers in Earth Science, 8, 652, https://doi.org/10.3389/feart.2020.608063, 2021a.
741
742 Bello, S., Scott, C. P., Ferrarini, F., Brozzetti, F., Scott, T., Cirillo, D., de Nardis R., Arrowsmith R. J., and Lavecchia G.:
743 High-resolution surface faulting from the 1983 Idaho Lost River Fault Mw 6.9 earthquake and previous events. Sci. Data 8,
744 68, 1-20, https://doi.org/10.1038/s41597-021-00838-6, 2021b.
745
746 Blumetti, A. M., Esposito, E., Ferreli, L., Michetti, A. M., Porfido, S., Serva, L., et al.: New data and the reinterpretation of
747 the november 23, 1980, M 6.9, Irpinia-Lucania earthquake (Southern Apennines) coseismic surface effects, Spec. Issue Studi
748 Geologici Camerti 2, 19-27, 2002.
749
750 Bousquet, J.C., and Gueremy, P.: Quelques Phénomènes de Néotectonique dans l'Apennin Calabro-Lucanien et Leurs
751 Conséquences Morphologiques. Rev. Géogr. Phys. Géol. Dynam 10, 225-238, 1969.

Bousquet, J.C.: La tectonique tangentielle des series calcareo-dolomitiques du nord est de l'apennin Calabro-Lucanien (Italie Méridionale). Geol. Rom. X, 23-52, 1971.

Brozzetti, F., and Lavecchia, G.: Seismicity and related extensional stress field: the case of the Norcia Seismic Zone (Central Italy), Ann. Tectonicae, 8(1), 36-57, 1994.

Brozzetti, F., Lavecchia, G., Mancini, G., Milana G. and Cardinali, M.: Analysis of the 9 September 1998 Mw 5.6 Mercure earthquake sequence (southern Apennines, Italy): a multidisciplinary approach, Tectonophysics, 476, 210-225. https://doi.org/10.1016/j.tecto.2008.12.007, 2009.

Brozzetti, F.: The Campania-Lucania extensional fault system (southern Italy): a suggestion for a uniform model of active extension in the Italian Apennines, Tectonics, 30 (5), 1-26, TC5009, http://dx.doi.org/10.1029/2010TC002794, 2011.

Brozzetti, F., Cirillo, D., de Nardis, R., Cardinali, M., Lavecchia, G., Orecchio, B., Presti D., and Totaro, C.: Newly identified active faults in the Pollino seismic gap, southern Italy, and their seismotectonic significance, J. Struct. Geol., 94, 13-31, https://doi.org/10.1016/j.jsg.2016.10.005, 2017a.

Brozzetti, F., Cirillo, D., Liberi, F., Piluso, E., Faraca, E., De Nardis, R., and Lavecchia, G.: Structural style of Quaternary extension in the Crati Valley (Calabrian Arc): Evidence in support of an east-dipping detachment fault, It. Journ. of Geosci., 136(3), 434-453, https://doi.org/10.3301/IJG.2017.11, 2017b.

Caiazzo, C., Giovine, B., Ortolani, F., Pagliuca, S., Schiattarella, M., andbarchi Vitale, C. : Genesi ed evoluzione strutturale della depressione tettonica dell'alta valle del Fiume Sele (Appennino Campano Lucano), Stud. Geol. Camerti, 1992(1), 245–255, 1992.

Calamita, F., Pizzi, A., and Roscioni, M.: I fasci di faglie recenti ed attive di M. Vettore - M. Bove e di M. Castello - M. Cardosa (Appennino Umbro-Marchigiano), In Studi Geologici Camerti; Università di Camerino: Camerino, Italy, 81-95, 1992; Available online: http://193.204.8.201:8080/jspui/handle/1336/552, last access: 19 April 2021.

Castaldo, R., de Nardis, R., De Novellis, V., Ferrarini, F., Lanari, R., Lavecchia, G., et al.: Coseismic stress and strain field changes investigation through 3-D Finite Element modeling of DInSAR and GPS measurements and geological/seismological data: the l'aquila (Italy) 2009 earthquake case study, J. Geophys. Res. Solid Earth 123, 4193-4222, https://doi.org/10.1002/2017JB014453, 2018.

https://doi.org/10.5194/se-2021-76
Preprint. Discussion started: 11 June 2021

786
787 Castello, B., Selvaggi, G., Chiarabba, C., and Amato, A.: CSI Catalogo della sismicità italiana 1981-2002, versione 1.1. Roma:
788 INGV-CNT, 2006, https://csi.rm.ingv.it/, last access: 19 April 2021.
789
790 Cello, G., Tondi, E., Micarelli, L., and Mattioni L.: Active tectonics and earthquake sources in the epicentral area of the 1857
791 Basilicata earthquake (southern Italy), Journal of Geodynamics, 36, 1-2, 37-50, https://doi.org/10.1016/S0264-3707(03)00037-
792 1, 2003.
793
794 Cheloni, D., D'Agostino, N., Selvaggi, G., Avallone, A., Fornaro, G., Giuliani, R., Reale, D., Sansosti, E., and Tizzani, P.,:
795 Aseismic transient during the 2010–2014 seismic swarm: evidence for longer recurrence of Ml ≥6.5 earthquakes in the Pollino
796 gap (Southern Italy)?, Sci. Rep., 7(576), https://doi.org/10.1038/s41598-017-00649-z, 2017.
797
798 Chiaraluce, L., Amato, A., Cocco, M., Chiarabba, C., Selvaggi, G., Di Bona, M., Piccinini, D., Deschamps, A., Margheriti, L.,
799 Courboulex, F., and Ripepe, M.: Complex normal faulting in the Apennines thrust-and-fold belt: The 1997 seismic sequence
800 in Central Italy, Bull. Seismol. Soc. Am. 94, 99-116, https://doi.org/10.1785/0120020052, 2004.
801
802 Chiaraluce, L., Barchi, M.R., Collettini, C., Mirabella, F., and Pucci, S.: Connecting seismically active normal faults with
803 Quaternary geological structures: the Colfiorito 1997 case history (Northern Apennines, Italy), Tectonics 24, TC1002, 1-16,
804 https://doi.org/10.1029/2004TC001627, 2005.
805
806 Chiaraluce, L., Valoroso, L., Piccinini, D., Di Stefano, R., and De Gori, P.: The anatomy of the 2009 L'Aquila normal fault
807 system (central Italy) imaged by high resolution foreshock and aftershock locations, J. Geophys. Res. 116, no. B12,
808 https://doi.org/10.1029/2011JB008352, 2011.
809
810 Chiaraluce, L., Di Stefano, R., Tinti, E., Scognamiglio, L., Michele, M., Casarotti, E., Cattaneo, M., De Gori, P., Chiarabba,
811 C., Monachesi, G., Lombardi, A., Valoroso, L., Latorre, D., and Marzorati, S.: The 2016 Central Italy Seismic Sequence: A
812 First Look at the Mainshocks, Aftershocks, and Source Models, Seismological Research Letters, 88(3), 757-771,
813 https://doi.org/10.1785/0220160221, 2017.
814
815 Cinque, A., Patacca, E., Scandone, P., and Tozzi, M.: Quaternary kinematic evolution of the southern apennines. relationship
816 between surface geological features and lithospheric structures, Ann. Geofisc 36, 249–260. https://doi.org/10.4401/ag-4283,
817 1993.
818

819 Cinque, A., Ascione, A., and Caiazzo, C.:Distribuzione spaziotemporale e caratterizzazione della fagliazione quaternaria in
820 Appennino meridionale, in Le Ricerche del GNDT nel Campo Della Pericolosità Sismica (1996–1999), edited by F. Galadini,
821 C. Meletti, and A. Rebez, 397 pp., CNR, Gruppo Naz. per la Difesa dai Terremoti, Rome, 2000.
822
823 Cinti, F. R., Cucci, L., Pantosti, D., D'Addezio, G., and Meghraoui, M.: A major seismogenic fault in a 'silent area': the
824 Castrovillari fault (southern Apennines, Italy), Geophysical Journal International, 130(3), 595-605, 1997. https://www.earth-
825 prints.org/bitstream/2122/12031/1/text.pdf, last access: 19 April 2021.
826
827 Cinti, F. R., Moro, M., Pantosti, D., Cucci, L., and D'Addezio, G.: New constraints on the seismic history of the Castrovillari
828 fault in the Pollino gap (Calabria, southern Italy), J. Seismol., 6, 199-217. https://doi.org/10.1023/A:1015693127008, 2002.
829
830 Cirillo, D.: Digital Field Mapping and Drone-Aided Survey for Structural Geological Data Collection and Seismic Hazard
831 Assessment: Case of the 2016 Central Italy Earthquakes, Applied Sciences, 10, 5233. https://doi.org/10.3390/app10155233,
832 2020.
833
834 D'Agostino, N.: Complete seismic release of tectonic strain and earthquake recurrence in the Apennines (Italy), Geophys. Res.
835 Lett 41, 1155-1162, https://doi.org/10.1002/2014GL059230, 2014.
836
837 D'Alessandro, A., Gervasi, A., and Guerra, I.: Evolution and strengthening of the Calabrian regional seismic network. Adv.
838 Geosciences 36, 11-16, 2013. https://adgeo.copernicus.org/articles/36/11/2013/adgeo-36-11-2013.pdf, last access: 19 April
839 2021.
840
841 D'Argenio, B.: L'Appennino Campano Lucano. Vecchi e nuovi modelli geologici tra gli anni sessanta e gli inizi degli anni
842 ottanta. Mem. Soc. Geol. It. 41, 3-15, 1992.
843
844 Delvaux, D., and Sperner, B.: New aspects of tectonic stress inversion with reference to the TENSOR program. In: New
845 Insights into Structural Interpretation and Modelling (D.A. Nieuwland, ed.), J. Geol. Soc. London Spec. Publ., 212, 75-100,
846 2003.
847
848 Delvaux, D., and Barth, A.: African stress pattern from formal inversion of focal mechanism data, Tectonophysics, 482, 105-
849 128, 2010.
850

851 Di Bucci, D., Buttinelli, M., D'Ambrogi, C., and Scrocca, D., and the RETRACE-3D Working Group: The RETRACE-3D
852 multi-data and multi-expertise approach towards the construction of a 3D crustal model for the 2016-2018 Central Italy seismic
853 sequence, Boll. Geof. Teor. Appl. DOI 10.4430/bgta0343, 2021.
854
855 Elter, P., Giglia, G., Tongiorgi, M., and L. Trevisan, L.: Tensional and compressional areas in the recent (Tortonian to present)
856 evolution of the northern Apennines, Boll. Geofis. Teor. Appl., 17, 3-18, 1975.
857
858 Ercoli, M., Pauselli, C., Forte, E., Frigeri, A., and Federico, C.: The Mt. Pollino Fault (southern Apennines, Italy): GPR
859 signature of Holocenic earthquakes in a "silent" area. In: Advanced Ground Penetrating Radar (IWAGPR), 2013 7th
860 International Workshop. IEEE, pp. 1-6. http://dx.doi.org/10.1109/IWAGPR.2013.6601510, 2013.
861
862 Ercoli M., Cirillo D., Pauselli C., Jol H. M., and Brozzetti F.: GPR signature of Quaternary faulting: a study from the Mt.
863 Pollino region, southern Apennines, Italy, submitted this special issue Solid Earth, 2021.
864
865 Faure Walker, J. P., Roberts, G. P., Cowie, P. A., Papanikolaou, I., Michetti, A. M., Sammonds, P., et al.: Relationship between
866 topography, rates of extension and mantle dynamics in the actively-extending italian apennines, Earth Planet Sci. Lett 325–
867 326, 76–84. doi:10.1016/j.epsl.2012.01.028, 2012.
868
869 Ferranti, L., Milano, G., and Pierro, M., Insights on the seismotectonics of the western part of northern Calabria (southern
870 Italy) by integrated geological and geophysical data: coexistence of shallow extensional and deep strike-slip kinematics,
871 Tectonophysics, 721, 372–386, https://doi.org/10.1016/j.tecto.2017.09.020, 2017.
872
873 Ferrarini, F., Lavecchia, G., de Nardis, R., and Brozzetti, F.: Fault geometry and active stress from earthquakes and field
874 geology data analysis: the Colfiorito 1997 and L'Aquila 2009 cases (central Italy), Pure Appl. Geoph., 172 (5), 1079-1103,
875 https://doi.org/10.1007/s00024-014-0931-7, 2015.
876
877 Filice, F., Liberi, F., Cirillo, D., Pandolfi, L., Marroni, M., and Piluso E.: Geology map of the central area of Catena Costiera:
878 insights into the tectono-metamorphic evolution of the Alpine belt in Northern Calabria, Journal of Maps, 11(1), 114-125,
879 https://doi.org/10.1080/17445647.2014.944877, 2015.
880
881 Filice, F., and Seeber, L.: The Culmination of an Oblique Time-Transgressive Arc Continent Collision: The Pollino Massif
882 Between Calabria and the Southern Apennines, Italy, Tectonics, 38(1), 3261-3280. https://doi.org/10.1029/2017TC004932,
883 2019.
884

885 Frepoli, A., Cinti, R., Amicucci, L., Cimini, G.B., De Gori, P., and Pierdominici, S.: Pattern of seismicity in the Lucanian
886 Apennines and foredeep (Southern Apennines) from recording by SAPTEX temporary array, Annal. Geophys., 48, 1035-1054,
887 2005. https://www.earth-prints.org/bitstream/2122/1131/6/manuscript.pdf , last access: 19 April 2021.
888
889 Frohlich, C.: Display and quantitative assessment of distributions of earthquakes focal mechanisms, Geophys. J. Int. 144, 300-
890 308, 2001.
891
892 Gafarov, K., Ercoli, M., Cirillo, D., Pauselli, C., and Brozzetti, F.: Extending surface geology data through GPR prospections:
893 Quaternary faulting signature from the Campotenese area (Calabria-Italy), 17th International Conference on Ground
894 Penetrating Radar, GPR, 8441611, 2018.
895
896 Galadini, F., and P. Galli: Active tectonics in the Central Apennines (Italy): Input data for seismic hazard assessment, Nat.
897 Hazards, 22, 225–268, doi:10.1023/A:1008149531980, 2000.
898
899 Galli, P., and Peronace, E.: New paleoseismic data from the Irpinia fault. A different seismogenic perspective for the southern
900 Apennines, Earth Sci. Rev. 136, 175-201, https://doi.org/10.1016/j.earscirev.2014.05.013, 2014.
901
902 Galli, P.: Recurrence times of central-southern Apennine faults (Italy): Hints from paleoseismology, Terra Nova, 32, 399-407,
903 https://doi.org/10.1111/ter.12470, 2020.
904
905 Gephart, J.W., and Forsyth, D.W.: An improved method for determining the regional stress tensor using earthquake focal
906 mechanism data: application to the San Fernando earthquake sequence, J. Geophys. Res., 89, 9305-9320, 1984.
907
908 Ghisetti, F., and Vezzani, L.: Strutture tensionali e compressive indotte da meccanismi profondi lungo la linea del Pollino
909 (Appennino meridionale), Boll. Soc.Geol. It. 101, 385-440, 1982.
910
911 Ghisetti, F., and Vezzani, L.: Structural Map of Mt. Pollino (Southern Italy), 1:50.000 Scale, SELCA, Firenze,1983.
912
913 Giano, S. I., and Martino, C.: Assetto morfotettonico e morfostratigrafico di alcuni depositi continentali pleistocenici del bacino
914 del pergola–melandro (Appennino Lucano). Quaternario 16 (2), 289–297, 2003.
915
916 Grandjacquet, C.: Données nouvelles sur la tectonique tertiaire des massif Calabro-Lucaniens. Bull. Soc. Geol. Fr. 7ème série
917 4, 695-706, 1962.
918

Guerra, I., Harabaglia, P., Gervasi, A., and Rosa, A.B.: The 1998–1999 Pollino (Southern Apennines, Italy) seismic crisis: tomography of a sequence, Ann. Geophys. 48, 995-1007, https://doi.org/10.4401/ag-3249, 2005.

Guidoboni E., Ferrari G., Mariotti D., Comastri A., Tarabusi G., Sgattoni G., and Valensise G.: CFTI5Med, Catalogo dei Forti Terremoti in Italia (461 a.C.-1997) e nell'area Mediterranea (760 a.C.-1500), Istituto Nazionale di Geofisica e Vulcanologia (INGV), http://storing.ingv.it/cfti/cfti5/, 2018.

Guidoboni, E., Ferrari, G., Tarabusi, G., Sgattoni, G., Comastri, A., Mariotti, D., Ciuccarelli, C., Bianchi, M.G., and Valensise G.: CFTI5Med, the new release of the catalogue of strong earthquakes in Italy and in the Mediterranean area, Scientific Data 6, Article number: 80, doi: https://doi.org/10.1038/s41597-019-0091-9, 2019.

Heidbach, O., Tingay, M., Barth, A., Reinecker, J., Kurfeß, D., and Müller, B.: Global crustal stress pattern based on the world stress map database release 2008, Tectonophysics 482, 3-15, https://doi.org/10.1016/j.tecto.2009.07.023, 2010.

Hippolite, J.C., Angelier, J., and Barrier, E.: Compressional and extensional tectonics in an arc system; example of the Southern Apennines, J. Struct. Geol. 17, 1725–1740, https://doi.org/10.1016/0191-8141(95)00066-M, 1995.

Husen, S., and Smith, R.: Probabilistic earthquake location in three dimensional velocity models for the Yellowstone National Park region, Wyoming, Bull. Seism. Soc. Am. 94 (6), 880-896, 2004. https://uusatrg.utah.edu/PAPERS/husen2004probeqreloc.pdf, last access: 19 April 2021.

Iannace, A., D'Errico, M., and Vitale, S.: Carta Geologica dell'area compresa tra Maratea, Castrovillari e Sangineto. In: Vitale, S., Iannace, A. (Eds.), Analisi Dello Strain Finito in 3D Dell'Unità Pollino-Ciagola (Confine Calabro-lucano, Italia Meridionale), Studi Geologici Camerti, Nuova Serie, 2, 153-167 (ISSN: 0392-0631), 2004.

Iannace, A., Garcia Tortosa, F.J., and Vitale, S.: The Triassic metasedimentary successions across the boundary between Southern Apennines and Calabria–Peloritani Arc (Northern Calabria, Italy), Geol. J., 40, 155–171. https://doi.org/10.1002/gj.1001, 2005.

Iannace, A., Vitale, S., D'Errico, M., Mazzoli, S., Di Staso, A., Macaione, E., Messina, A., Reddy, S.M., Somma, R., Zamparelli, V., Zattin, M., and Bonardi, G.: The carbonate tectonic units of northern Calabria (Italy): a record of Apulian palaeomargin evolution and Miocene convergence, continental crust subduction, and exhumation of HP–LT rocks, J. Geol. Soc. Lond. 164, 1165-1186. https://doi.org/10.1144/0016-76492007-017, 2007.

953 Ietto, A., and Barilaro, A.M.: L'Unità di San Donato quale margine deformato Cretacico-Paleogene del bacino di Lagonegro
954 (Appennino Meridionale-Arco Calabro), Boll. Soc. Geol. It. 112, 477-496, 1993.
955
956 ISIDe Working Group: Italian Seismological Instrumental and Parametric Database (ISIDe). Istituto Nazionale di Geofisica e
957 Vulcanologia (INGV), https://doi.org/10.13127/ISIDE, 2007, last access: 19 April 2021.
958
959 Johnson, K., Nissen, E., Saripalli, S., Arrowsmith, J.R., McGarey, P., Scharer, K., Williams, P., Blisniuk, K.: Rapid mapping
960 of ultrafine fault zone topography with structure from motion, Geosphere, 10, 969–986, 2014.
961
962 Knott, S.D., and Turco, E.: Late cenozoic kinematics of the Calabrian arc, southern Italy. Tectonics 10 (6), 1164-1172, 1991.
963
964 Lavecchia, G., Brozzetti, F., Barchi, M., Menichetti, M., and Keller, J. V. A.: Seismotectonic zoning in east-central Italy
965 deduced from an analysis of the neogene to present deformations and related stress fields, Geol. Soc. Am. Bull. 106, 1170-
966 1120, doi:10.1130/0016, https://doi.org/10.1130/0016-7606(1994)106%3C1107:SZIECI%3E2.3.CO;2, 1994.
967
968 Lavecchia, G., Boncio, P., Brozzetti, F., De Nardis, R., Di Naccio, D., Ferrarini, F., Pizzi, A., and Pomposo, G.: The April
969 2009 L'Aquila (central Italy) seismic sequence (Mw 6.3): a preliminary seismotectonic picture, Recent Prog. Earthquake Geol.
970 2011, 1-17, ISBN: 978-1-60876-147-0, 2011.
971
972 Lavecchia, G., Ferrarini, F., Brozzetti, F., de Nardis, R., Boncio, P., and Chiaraluce, L.: From surface geology to aftershock
973 analysis: constraints on the geometry of the L'Aquila 2009 seismogenic fault system. Italian J. Geosciences 131 (3), 330-347,
974 2012.
975
976 Lavecchia G., de Nardis, R., Costa, G., Tiberi, L., Ferrarini, F., Cirillo, D., Brozzetti F., and Suhadolc, P.: Was the Mirandola
977 thrust really involved in the Emilia 2012 seismic sequence (northern Italy)? Implications on the likelihood of triggered
978 seismicity effects, Boll. Geof. Teor. Appl., Vol. 56, n. 4, pp. 461- 488, 2015.
979
980 Lavecchia, G., Castaldo, R., de Nardis, R., De Novellis, V., Ferrarini, F., Pepe, S., Brozzetti, F., Solaro, G., Cirillo, D., Bonano,
981 M., Boncio, P., Casi, F., De Luca, C., Lanar, R., Manunta, M., Manzo, M., Pepe, A., Zinno, I., and Tizzani, P.: Ground
982 deformation and source geometry of the 24 August 2016 Amatrice earthquake (Central Italy) investigated through analytical
983 and numerical modeling of DInSAR measurements and structural-geological data, Geophys. Res. Lett., 43,
984 https://doi.org/10.1002/2016GL071723, 2016
985

https://doi.org/10.5194/se-2021-76
Preprint. Discussion started: 11 June 2021

Lavecchia, G., Adinolfi, G. M., de Nardis, R., Ferrarini, F., Cirillo, D., Brozzetti, F., De Matteis, R., Festa, G., and Zollo, A.: Multidisciplinary inferences on a newly recognized active east-dipping extensional system in central Italy, Terra Nova, 29, 77–89, https://doi.org/10.1111/ter.12251, 2017.

Lavecchia, G., de Nardis, R., Ferrarini, F., Cirillo, D., Bello, S., and Brozzetti, F.: Regional seismotectonic zonation of hydrocarbon fields in active thrust belts: a case study from Italy, in Building knowledge for geohazard assessment and management in the caucasus and other orogenic regions, Editors F. L. Bonali, F. Pasquaré Mariotto, and N. Tsereteli (the Netherlands: Springer), doi:10.1007/978-94-024-2046-3, 2021.

Leonard, M.: Earthquake fault scaling: Relating rupture length, width, average displacement, and moment release, Bull. Seismol. Soc. Am., 100(5A), 1971-1988. https://doi.org/10.1785/0120090189, 2010.

Liberi, F., Morten, L., and Piluso, E.: Geodynamic significance of the ophiolites within the Calabrian Arc, Island Arc, 15, 26–43, 2006.

Liberi, F., and Piluso, E.: Tectonometamorphic evolution of the ophiolitic sequences from Northern Calabrian Arc, Italian Journal Geoscience (Bollettino Society Geological Italian), 128, 483–493, 2009.

Lippmann-Provansal, M.: L'Appennin meridionale (Italie): Etude geomorphologique, these Doctorat, Univ. d'Aix-Marseille II, Marseille, France, 1987.

Lomax, A., Virieux, J., Volant, P., and Berge-Thierry, C.: Probabilistic Earthquake Location in 3D and Layered Model, in Advances in Seismic Event Location, Pp. 101-134, Kluwer Academic Publishers, Netherlands, 2000.

Margheriti, L., Amato, A., Braun, T., Cecere, G., D'Ambrosio, C., De Gori, and P., Selvaggi, G.: Emergenza nell'area del Pollino: le attività della Rete Sismica Mobile, Rapporti Tecnici INGV, 2013.

Marrett, R. A., and Allmendinger, R. W.: Kinematic analysis of fault-slip data, Journal of Structural Geology, v. 12, p. 973-986, 1990.

Maschio, L., Ferranti, L., and Burrato, P.: Active extension in Val d'Agri area, southern Apennines, Italy: Implications for the geometry of the seismogenic belt, Geophys. J. Int., 162, 591–609, https://doi.org/10.1111/j.1365-246X.2005.02597.x., 2005.

1019 Michetti, A. M., Ferreli, L., Serva, L., and Vittori, E.: Geological evidence for strong historical earthquakes in an "aseismic"
1020 region: The Pollino case (Southern Italy), Journal of Geodynamics, 24:1-4, 67-86. https://doi.org/10.1016/S0264-
1021 3707(97)00018-5, 1997.
1022
1023 Michetti, A. M., Ferreli, L., Esposito, E., Porfido, S., Blumetti, A. M., Vittori, E., Serva, L., and Roberts, G. P.: Ground Effects
1024 during the 9 September 1998, Mw = 5.6 Lauria, Earthquake and the Seismic Potential of the seismic Pollino Region in Southern
1025 Italy, Seismological Research Letters, 71(1), 31-46. https://doi.org/10.1785/gssrl.71.1.31, 2000.
1026
1027 Montone, P., Mariucci, M.T., Pondrelli, S., Amato, A.: An improved stress map for Italy and surrounding regions (central
1028 Mediterranean), J. Geophys. Res. 109, B10410. http://dx.doi.org/10.410.11029/12003JB002703, 2004.
1029
1030 Montone, P., Mariucci, M.T., and Pierdominici, S.: The Italian present-day stress map, Geophys. J. Int., 189, 705- 716;
1031 https://doi.org/10.1111/j.1365-246X.2012.05391.x, 2012.
1032
1033 Mostardini, F., and Merlini, S.: Appennino centro meridionale - Sezioni geologiche e proposta di modello strutturale. Mem.
1034 Soc. Geol. Ital. 35, 177–202, 1986
1035
1036 Napolitano, F., De Siena, L., Gervasi, A., Guerra, I., Scarpa, R., and La Rocca, M.: Scattering and absorption imaging of a
1037 highly fractured fluid-filled seismogenetic volume in a region of slow deformation, Geosci. Front., 11(3), 989-998.
1038 https://doi.org/10.1016/j.gsf.2019.09.014, 2020.
1039
1040 Napolitano, F., Galluzzo, D., Gervasi, A., Scarpa, R., La Rocca, M.: Fault imaging at Mt Pollino (Italy) from relative location
1041 of microearthquakes, Geophysical Journal International, 224(1), 637-648, https://doi.org/10.1093/gji/ggaa407 , 2021.
1042
1043 Nicholson, G., Plesch, A., Sorlion, C. C., Shaw, J. H., and Hauksson, E.: TheSCEC 3D community fault model (CFM-v5): an
1044 updated and expanded fault set of oblique crustal deformation and complex fault interaction for southern California, Eos Trans.
1045 Am. Geophys. Union 95 (52). Abstract T31B-4584, 2014.
1046
1047 Nicholson, C., Plesch, A., Sorlien, C. C., Shaw, J. H., and Hauksson, E.: The SCEC community fault model version 5.0: an
1048 updated and expanded 3D fault set for southern California, in 2015 pacific section AAPG joint meeting program (Oxnard,
1049 CA), Vol. 77, September 12-16, 2015.
1050
1051 Ogniben, L.: Schema introduttivo alla geologia del confine calabro-lucano, Mem. Soc. Geol. It, 8, 453-763, 1969.
1052

1053 Ogniben, L.: Schema geologico della Calabria in base ai dati odierni, Geologia Romana, 12, 243–585, 1973.
1054
1055 Orecchio, B., Presti, D., Totaro, C., Guerra, I., and Neri, G.: Imaging the velocity structure of the Calabrian Arc region (south
1056 Italy) through the integration of different seismological data, Boll. Geofis. Teor. Appl. 52, 625-638, 2011,
1057 http://www3.ogs.trieste.it/bgta/pdf/bgta0023_ORECCHIO.pdf last access: 19 April 2021.
1058
1059 Pantosti, D., and Valensise, G.: Faulting mechanism and complexity of the november 23, 1980, campania-lucania earthquake,
1060 inferred from surface observation, J. Geophys. Res 95, 15319. doi:10.1029/jb095ib10p15319, 1990.
1061
1062 Pantosti, D., and Valensise, G.: Source geometry and long term behavior of the 1980, Irpinia earthquake fault based on field
1063 geologic observations. Ann. Geofisc 36, 41–49. https://doi.org/10.4401/ag-4299, 1993.
1064
1065 Papanikolaou, I. D., and Roberts, G. P.: Geometry, kinematics and deformation rates along the active normal fault system in
1066 the southern Apennines: implications for fault growth, J. Struct. Geol 29, 166-188. https://doi.org/10.1016/j.jsg.2006.07.009,
1067 2007.
1068
1069 Passarelli, L., Hainzl, S., Cesca, S., Meccaferri, F., Mucciarelli, M., Roessler, D., Corbi, F., Dahm, T., and Rivalta, E.: Aseismic
1070 transient driving the swarm-like seismic sequence in the Pollino range, Southern Italy, Geophys. J. Int., 201(3), 1553–1567,
1071 https://doi.org/10.1093/gji/ggv111, 2015.
1072
1073 Pastori, M., Margheriti, L., De Gori, P., Govoni, A., Lucente, F.P., Moretti, M., Marchetti, A., Di Giovambattista, R., Anselmi,
1074 M., De Luca, P., Nardi, A, Agostinetti, N.P., Latorre, D., Piccinini, D., Passarelli, L., and Chiarabba, C.: The 2011–2014
1075 Pollino Seismic Swarm: Complex Fault Systems,Imaged by 1D Refined Location and Shear Wave Splitting Analysis at the
1076 Apennines–Calabrian Arc Boundary, Front. Earth Sci. 9:618293. doi: 10.3389/feart.2021.618293, 2021.
1077
1078 Patacca, E., and Scandone, P.: Geological interpretation of the CROP-04 seismic line (Southern Apennines, Italy), Boll. Soc.
1079 Geol. It. (Ital. J. Geosci.), 7, 297-315, 2007.
1080
1081 Plesch, A., Shaw, J. H., and Jordan, T. H.: Stochastic descriptions of basin velocity structure from analyses of sonic logs and
1082 the SCEC community velocity model (CVM-H), in Presentation at 2014 SSA annual meeting, Palm Springs, CA, September
1083 6-10, 2014.
1084
1085 Pondrelli, S., Salimbeni, S., Ekström, G., and Morelli, A.: The Italian CMT dataset from 1977 to the present, Phys. Earth
1086 Planet, In 159, 286–303, https://doi.org/10.1016/j.pepi.2006.07.008, 2006.

1087

1088 Presti, D., Troise, C., and De Natale, G.: Probabilistic location of seismic sequences in heterogeneous media, Bull. Seismol.
1089 Soc. Am. 94, 2239-2253, DOI: 10.1785/0120030160, 2004.

1090

1091 Presti, D., Orecchio, B., Falcone, G., and Neri, G.: Linear versus nonlinear earthquake location and seismogenic fault detection
1092 in the southern Tyrrhenian Sea. Italy, Geophys. J. Int. 172, 607-618, https://doi.org/10.1111/j.1365-246X.2007.03642.x, 2008.

1093

1094 Robustelli, G., Russo Ermolli, E., Petrosino, P., Jicha, B., Sardella, R., and Donato, P.: Tectonic and climatic control on
1095 geomorphological and sedimentary evolution of the Mercure basin, southern Apennines, Italy, Geomorphology 214, 423-435,
1096 https://doi.org/10.1016/j.geomorph.2014.02.026, 2014.

1097

1098 Rovida, A., Locati, M., Camassi, R., Lolli, B., and Gasperini, P.: The Italian earthquake catalogue CPTI15, Bulletin of
1099 Earthquake Engineering, 18, 2953-2984, https://doi.org/10.1007/s10518-020-00818-y, 2020.

1100

1101 Rovida A., Locati M., Camassi R., Lolli B., Gasperini P., and Antonucci A.: Catalogo Parametrico dei Terremoti Italiani
1102 (CPTI15), versione 3.0. Istituto Nazionale di Geofisica e Vulcanologia (INGV). https://doi.org/10.13127/CPTI/CPTI15.3,
1103 2021.

1104

1105 SCEC, 2021 https://www.scec.org/research/cfm;

1106

1107 Schiattarella, M., Torrente, M., and Russo, F.: Analisi strutturale ed osservazioni morfotettoniche nel bacino del Mercure
1108 (Confine calabro-lucano), Il Quaternaio, 7, 613-626, 1994.

1109

1110 Scognamiglio, L., Tinti, E., and Quintiliani, M.: Time Domain Moment Tensor (TDMT) [Data set]. Istituto Nazionale di
1111 Geofisica e Vulcanologia (INGV). https://doi.org/10.13127/TDMT, 2006.

1112

1113 Servizio Geologico d'Italia: 220 Verbicaro Sheet of the Carta Geologica D'Italia, 1. 100.000 Scale. Rome, 1970.

1114

1115 Sgambato, C.,Walker, J. P. F., and Roberts, G. P.: Uncertainty in strain-rate from field measurements of the geometry, rates
1116 and kinematics of active normal faults: implications for seismic hazard assessment, J. Struct. Geol 131,
1117 103934.doi:10.1016/j.jsg.2019.103934, 2020.

1118

1119 Sperner, B., Müller, B., Heidbach, O., Delvaux, D., Reinecker, J., and Fuchs, K.: Tectonic stress in the Earth's crust: advances
1120 in the World Stress Map project. In: New Insights into Structural Interpretation and Modelling (D.A. Nieuwland, ed.), J. Geol.
1121 Soc. London Spec. Publ., 212, 101–116, https://doi.org/10.1144/GSL.SP.2003.212.01.07, 2003.
1122
1123 Spina, V., Galli, P., Tondi, E., and Mazzoli, S.: Fault propagation in a seismic gap area (northern Calabria, Italy): implications
1124 for seismic hazard, Tectonophysics, 476, 357-369, https://doi.org/10.1016/j.tecto.2009.02.001, 2009.
1125
1126 Stirling, M., Goded, T., Berryman, K. and Litchfield, N.: Selection of Earthquake Scaling Relationships for Seismic-Hazard
1127 Analysis, Bulletin of the Seismological Society of America, 103(6), 2993-3011. https://doi.org/10.1785/0120130052, 2013.
1128
1129 Tangari, A.C., Scarciglia, F., Piluso, E., Marinangeli, L., and Pompilio, L.: Role of weathering of pillow basalt, pyroclastic
1130 input and geomorphic processes on the genesis of the Monte Cerviero upland soils (Calabria, Italy), Catena, 171, 299-315,
1131 ISSN 0341-8162, https://doi.org/10.1016/j.catena.2018.07.015, 2018.
1132
1133 Tarquini, S., Vinci, S., Favalli, M., Doumaz, F., Fornaciai, A., and Nannipieri, L.: Release of a 10-m-resolution DEM for the
1134 Italian territory: Comparison with global-coverage DEMs and anaglyph-mode exploration via the web, Computers and
1135 Geosciences, 38, 168-170. https://doi.org/10.1016/j.cageo.2011.04.018, 2012.
1136
1137 TDMT database – INGV http://cnt.rm.ingv.it/tdmt.
1138
1139 Tertulliani, A., and Cucci, L.: New insights on the strongest historical earthquake in the Pollino region (southern Italy),
1140 Seismol. Res. Lett., 85(3), 743-751, https://doi.org/10.1785/0220130217, 2014.
1141
1142 Totaro, C., Presti, D., Billi, A., Gervasi, A., Orecchio, B., Guerra, I., and Neri, G.: The ongoing seismic sequence at the Pollino
1143 Mountains, Italy. Seismol. Res. Let., 84(6), 955-962, https://doi.org/10.1785/0220120194, 2013.
1144
1145 Totaro, C., Koulakov, I., Orecchio, B., and Presti, D.: Detailed crustal structure in the area of the southern Apennines–Calabrian
1146 Arc border from local earthquake tomography, J. Geodyn., 82, 87-97, https://doi.org/10.1016/j.jog.2014.07.004, 2014.
1147
1148 Totaro, C., Seeber, L., Waldhauser, F., Steckler, M., Gervasi, A., Guerra, I., Orecchio, B., and Presti, D.: An intense earthquake
1149 swarm in the southernmost Apennines: fault architecture from high-resolution hypocenters and focal mechanisms, Bull.
1150 Seismol. Soc. Am. 105, 1-6. https://doi.org/10.1785/0120150074, 2015.
1151

1152 Totaro, C., Orecchio, B., Presti, D., Scolaro, S., and Neri G.: Seismogenic stress field estimation in the Calabrian Arc region
1153 (south Italy) from a Bayesian approach, Geophys. Res. Lett., 43, 8960–8969, https://doi.org/10.1002/2016GL070107, 2016.
1154
1155 Valoroso, L., Chiaraluce, L., Di Stefano, R., and Monachesi, G.: Mixed-Mode Slip Behavior of the Altotiberina Low-Angle
1156 Normal Fault System (Northern Apennines, Italy) through High-Resolution Earthquake Locations and Repeating Events, J.
1157 Geoph. Res. Solid Earth, 122(12), 10220-10240, https://doi.org/10.1002/2017JB014607, 2017.
1158
1159 Van Dijk, J.P., Bello, M., Brancaleoni, G.P., Cantarella, G., Costa, V., Frixa, A., Golfetto, F., Merlini, S., Riva, M., Toricelli,
1160 S., Toscano, C., and Zerilli, A.: A regional structural model for the northern sector of the Calabrian Arc (southern Italy),
1161 Tectonophysics 324, 267-320, https://doi.org/10.1016/S0040-1951(00)00139-6, 2000.
1162
1163 Vezzani, L., Festa, A., and Ghisetti, F.C.: Geology and tectonic evolution of the Central-Southern Apennines, Italy, Special
1164 Paper of the Geological Society of America, 469, 1-58, https://doi.org/10.1130/SPE469, 2010.
1165
1166 Villani, F., and Pierdominici, S.: Late Quaternary tectonics of the Vallo di Diano basin (southern Apennines, Italy), Quat. Sci.
1167 Rev., 29, 3167-3183. https://doi.org/10.1016/j.quascirev.2010.07.003, 2010
1168
1169 Waldhauser F., and Ellsworth W.: A Double-Difference Earthquake Location Algorithm: Method and Application to the
1170 Northern Hayward Fault, California, Bull. Seism. Soc. Am. 90(6):1353-1368, http://dx.doi.org/10.1785/0120000006, 2000.
1171
1172 Waldhauser, F.: HypoDD: a Computer Program to Compute Double Difference Earthquake Locations. U.S. Geol. Surv, Menlo
1173 Park, California, pp. 01-113. Open-File Report, 2001.
1174
1175 Wells, D.L., and Coppersmith, K.J.: New empirical relationships among magnitude, rupture length, rupture width, rupture
1176 area, and surface displacement, Bull. Seismol. Soc. Am., 84(4), 974-1002, 1994.
1177
1178 Wesnousky, S.G.: Displacement and geometrical characteristics of earthquake surface ruptures: Issues and implications for
1179 seismic hazard analysis and the process of earthquake rupture, Bull. Seismol.Soc. Am., 98(4), 1609-1632.
1180 https://doi.org/10.1785/0120070111, 2008.
1181
1182 Westoby, M.J., Brasington, J., Glasser, N.F., Hambrey, M.J., and Reynolds, J.M.: 'Structure-from-motion' photogrammetry:
1183 A low-cost, effective tool for geoscience applications, Geomorphology, 179, 300–314, 2012.